Journal of Experimental Botany, Vol. 71, No. 1 pp. 138–153, 2020
doi:10.1093/jxb/erz407 Advance Access Publication September 19, 2019
This paper is available online free of all access charges (see https://academic.oup.com/jxb/pages/openaccess for further details)

RESEARCH PAPER

Overexpression of *HvCslF6* in barley grain alters carbohydrate partitioning plus transfer tissue and endosperm development

Wai Li Lim[1,2], Helen M. Collins[1,2], Caitlin S. Byrt[1,2,*], Jelle Lahnstein[1,2], Neil J. Shirley[1,2], Matthew K. Aubert[1,2], Matthew R. Tucker[1,2], Manuela Peukert[3,†], Andrea Matros[3,*] and Rachel A. Burton[1,2,‡]

[1] Australian Research Council Centre of Excellence in Plant Cell Walls, University of Adelaide, Waite Campus, Urrbrae, SA, Australia
[2] School of Agriculture, Food and Wine, University of Adelaide, Waite Campus, Urrbrae, SA, Australia
[3] Applied Biochemistry Group, Leibniz Institute of Plant Genetics and Crop Plant Research Stadt Seeland, Gatersleben, Germany

* Present address: Australian Research Council Centre of Excellence in Plant Energy Biology, University of Adelaide, Waite Campus, Urrbrae, SA, Australia.
† Present address: Federal Research Institute of Nutrition and Food, Department of Safety and Quality of Meat, Kulmbach, Bavaria, Germany.
‡ Correspondence: rachel.burton@adelaide.edu.au

Received 8 April 2019; Editorial decision 30 August 2019; Accepted 6 September 2019

Editor: Gwyneth Ingram, CNRS/Ecole Normale Superieure de Lyon, France

Abstract

In cereal grain, sucrose is converted into storage carbohydrates: mainly starch, fructan, and mixed-linkage (1,3;1,4)-β-glucan (MLG). Previously, endosperm-specific overexpression of the *HvCslF6* gene in hull-less barley was shown to result in high MLG and low starch content in mature grains. Morphological changes included inwardly elongated aleurone cells, irregular cell shapes of peripheral endosperm, and smaller starch granules of starchy endosperm. Here we explored the physiological basis for these defects by investigating how changes in carbohydrate composition of developing grain impact mature grain morphology. Augmented MLG coincided with increased levels of soluble carbohydrates in the cavity and endosperm at the storage phase. Transcript levels of genes relating to cell wall, starch, sucrose, and fructan metabolism were perturbed in all tissues. The cell walls of endosperm transfer cells (ETCs) in transgenic grain were thinner and showed reduced mannan labelling relative to the wild type. At the early storage phase, ruptures of the non-uniformly developed ETCs and disorganization of adjacent endosperm cells were observed. Soluble sugars accumulated in the developing grain cavity, suggesting a disturbance of carbohydrate flow from the cavity towards the endosperm, resulting in a shrunken mature grain phenotype. Our findings demonstrate the importance of regulating carbohydrate partitioning in maintenance of grain cellularization and filling processes.

Keywords: Barley, carbohydrate partitioning, cavity, fructan, (1,3;1,4)-β-glucan, grain morphology, starch, sucrose.

Abbreviations: DAP, days after pollination; DP, degree of polymerization; ETC, endosperm transfer cell; 1-FEH, fructan 1-exohydrolase; 6-FEH, fructan 6-exohydrolase; 1-FFT, fructan:fructan-1-fructosyltransferase; 6G-FFT, fructan:fructan-6G-fructosyltransferase; GBSS, granule-bound starch synthase; HPAEC–PAD, high pH anion exchange chromatography with pulsed amperometric detection; HvCslF6, cellulose synthase-like gene F6; HvCslH1, cellulose synthase-like gene H1; HvCslJ, cellulose synthase-like gene J; ISO, isoamylase; LD, limit dextrinase; MALDI-MSI, matrix-assisted laser desorption/ionization mass spectrometry imaging; MLG, mixed-linkage (1,3;1,4)-β-glucan; NP, nucellar projection; pAsGlo1, oat globulin AsGlo1 promoter sequence; SBE, starch branching enzyme;6-SFT, sucrose:fructan-6-fructosyltransferase; SS, starch synthase; 1-SST, sucrose:sucrose-1-fructosyltransferase;WT, wild type; WT(tc), wild type regenerated from tissue culture.

Introduction

The major storage carbohydrates in cereal grains include starch, fructan, and mixed linkage (1,3;1,4)-β-glucan (MLG). In *Hordeum vulgare* L. (barley) grain, starch represents the dominant storage polysaccharide contributing between 52% and 72% of the dry weight (Henry, 1988). In contrast, fructan constitutes 1–4% and MLG 4–10% of the total dry weight (Åman *et al.*, 1985; Henry and Saini, 1989; Burton and Fincher, 2012; Nemeth *et al.*, 2014). Changing carbohydrate metabolic pathways significantly influences grain development and final composition, and thus represents a key factor for future development of barley varieties with application-specific grain quality. In addition, the need to lower processing costs and reduce wastage of valuable nutrients, such as nutrients lost during pearling, have resulted in greater interest in hull-less barley varieties.

Allocation of carbohydrate occurs as soon as the grain begins to form and continues throughout development. At the pre-storage phase [0–6 days after pollination (DAP)], the maternal pericarp, besides its own chloroplast activities, receives additional sucrose from vascular tissue; this sucrose undergoes conversion to hexose sugars which are then used for transient starch reserves (Radchuk *et al.*, 2009; Sreenivasulu *et al.*, 2010). Concurrently, the maternal nucellus begins to disintegrate partly to support cell division and cellularization events in the early endosperm at 3 DAP (Sreenivasulu *et al.*, 2010; Domínguez and Cejudo, 2014). MLG is first deposited in the earliest cell walls at 4–5 DAP (Kohorn *et al.*, 2006), and oligofructans are detected in the vacuoles (Wagner and Wiemken, 1986). From 6 to 8 DAP, genes related to energy production and storage are expressed (Wobus *et al.*, 2005; Sreenivasulu *et al.*, 2010). Maintaining cytosolic sucrose homeostasis is indispensable for correct starch synthesis. Starch storage in the endosperm begins at 9 DAP (Olsen, 2001; Sreenivasulu *et al.*, 2010), coinciding with a high sucrose to hexose ratio (Wobus *et al.*, 2005).

Starch biosynthesis enzymes include granule-bound starch synthase (GBSS), starch synthase (SS), isoamylase (ISO), limit dextrinase (LD), starch branching enzyme (SBE), and ADP-glucose pyrophosphorylase (Radchuk *et al.*, 2009; Jeon *et al.*, 2010; Keeling and Myers, 2010). Fructans are synthesized by sucrose:sucrose-1-fructosyltransferase (1-SST), fructan:fructan-1-fructosyltransferase (1-FFT), sucrose:fructan-6-fructosyltransferase (6-SFT), and fructan:fructan-6G-fructosyltransferase (6G-FFT). Hydrolysis of fructans is mediated by fructan 1-exohydrolase (1-FEH) and fructan 6-exohydrolase (6-FEH) (Vijn and Smeekens, 1999). MLG accounts for 70% of cell wall material in barley endosperm (Fincher, 1975; Guillon *et al.*, 2011; Burton and Fincher, 2014), and MLG synthesis requires cellulose synthase-like enzymes HvCslF6, HvCslH1, and HvCslJ (Doblin *et al.*, 2009; Burton *et al.*, 2011; Little *et al.*, 2018) in balance with (1,3;1,4)-β-glucanase (Hrmova and Fincher, 2001).

Manipulation of genes associated with these pathways is a common strategy to produce crops with the desired grain composition. This manipulation can have a significant influence on grain development and composition. For example, the M292 mutation in the *starch synthase IIa* (*SSIIa*) gene produced a shrunken grain phenotype, with a reduction in starch content coinciding with significantly increased sucrose, fructan, and MLG content (Clarke *et al.*, 2008). The same phenotype was reported for low-starch barley lines with RNAi suppression of all starch branching enzyme genes (Carciofi *et al.*, 2012). It has been suggested that reduced metabolic uptake of sucrose in the endosperm transfer cell (ETC) region can cause an excessive accumulation of fluid that enlarges the grain cavity, resulting in shrunken grain after desiccation (Carciofi *et al.*, 2012; Shaik *et al.*, 2016). Larger grain cavities have previously been observed in barley lines overexpressing *HvCslF6*, and grain from these lines had higher MLG and reduced starch content. Morphological changes in these lines were detected in aleurone tissues that were on average three cell layers thick, with strongly defined walls and a pronounced cubic shape as well as deformed and, in places, completely missing transfer cells at the grain-filling phase (15 DAP). Mature transgenic grain had reduced size relative to control lines, a shrunken and darkened appearance, and increased brittleness (Lim *et al.*, 2018). In this study, we used transgenic grains overexpressing the *HvCslF6* gene as a model system to investigate the effects of increased MLG on carbohydrate metabolism, cavity formation, and cell identity during grain development.

Materials and methods

Plant materials

Barley plants were grown following Lim *et al.* (2018) under a day/night temperature regime of 23 °C/15 °C. Progeny of the T_3 generation from four independent transformed lines (15-3, 18-6, 25-5, and 16-5) overexpressing the *HvCslF6* gene were selected; these lines were referred to as lines F6-15, F6-18, F6-25, and F6-16 in Lim *et al.* (2018); in addition, Torrens [wild type (WT)] and WT plants regenerated from tissue culture [WT(tc)] were selected and analysed. Developing grains from individual plants were collected from the middle of the spike from 7 to 24 DAP at approximately mid-day, covering all phases of grain development. Mature grain was also collected. The 'outer tissues', endosperm, and embryo samples were separated using a scalpel and fine forceps, snap-frozen in liquid nitrogen, and kept at –80 °C until required. Experiments were performed on three biological replicates, consisting of at least 10 grains per replicate, with two technical replicates each, except where noted in the figure legend.

Vector construction and Agrobacterium-mediated barley transformation of pAsGlo1:3xnlsYFP

DNA fragments were synthesized by Genscript (USA) and inserted into the pUC57 vector. The 2.6 kb 3xnlsYFP gene (MA044) was adapted from Ueda *et al.* (2011) and codon optimized for barley using the online tool at https://sg.idtdna.com/CodonOpt (accessed 1 October 2019). The sequence for the 994 bp oat globulin AsGlo1 promoter sequence (pAsGlo1; MA003) was obtained from Vickers *et al.* (2006) and modified to include 5'-*Hin*dIII and 3'-*Kpn*I restriction sites. The *Hin*dIII/*Kpn*I pAsGlo1 fragment from MA003 was excised and inserted into the Gateway-compatible pMDC32 vector (Curtis and Grossniklaus, 2003) in place of the double 35S promoter, creating MA009. The 3xnlsYFP sequence was amplified from pUC57 using pUC57-attL1_FWD (5'-ACCTCGCGAATGCATCTAGATCA-3') and SacI-attL2_REV (5'-CAAATAATGATTTTATTTTGACTGATAGTGACCTGTTCG TTGCAACAAATTGATGAGCAATTATTTTTTATAATGCCAAC TTTGTACAAGAAAGCTGGGTTCATTATTTGGAGCTC-3') primers and HiFi Platinum Taq (Thermo Fisher Scientific), resulting in a PCR fragment flanked by attL1 and attL2 Gateway-compatible sites. The

3xnlsYFP insert was transferred into the MA009 (pAsGlo1:pMDC32) vector using LR clonase II (Thermo Fisher Scientific) according to the manufacturer's instructions. The resulting vector MA032 (pAsGlo1:3xnlsYFP) was transformed into *Agrobacterium tumefaciens* strain AGL1 and used for transformation of the *Hordeum vulgare* cv. WI4330 following the protocol outlined in Lim *et al.* (2018).

(1,3;1,4)-β-Glucan (MLG) assay

For the measurements of storage carbohydrates (MLG and starch) from developing and mature grain, the 'outer tissues' and the endosperm were analysed as a single sample. The embryo, containing low amounts of storage carbohydrates, was removed and used for analysis of soluble sugars. Freeze-dried samples were ground and weighed (10 mg). To remove free sugars and chlorophyll, samples were pre-treated with 70% ethanol (1 ml) at 97 °C for 30 min, centrifuged at 5000 rpm for 5 min, and supernatants removed. Pellets were washed with 100% ethanol (1 ml) at 97 °C for 10 min, centrifuged at 5000 rpm for 5 min, and supernatants removed. MLG content was measured using the Megazyme Mixed-linkage Beta-glucan Assay Kit (K-BGLU) (McCleary and Codd, 1991) as outlined in Lim *et al.* (2018).

Starch assay

Starch was measured using the Megazyme Total Starch Assay (AA/AMG) (McCleary *et al.*, 1994), with 10 mg of freeze-dried sample, pre-treated with 70% ethanol (30 min, 97 °C) and 100% ethanol (10 min, 97 °C).

Soluble sugar analysis

For the soluble sugar measurements, the developing and mature grains were separated into 'outer tissues', endosperm, and embryo tissue samples. Grains were ground and weighed (10 mg). Soluble sugars were extracted in 80% ethanol at 85 °C for 30 min followed by Milli-Q water at 50 °C for 30 min in a final dilution of 1:40 (w/v, mg μl^{-1}) and supernatants combined (Verspreet *et al.* (2012). For cavity sap, 10 barley grains were cut in half and fluids from the endosperm cavity were collected using a microsyringe (Hamilton). Cavity sap was immediately heated to 90 °C to inactivate endogenous enzymes and diluted in Milli-Q water to a final dilution of 1:100 (v/v). Extracts from grain tissues and cavity sap were treated or not with fructanase (Megazyme fructan assay kit, Deltagen), incubated at 40 °C for 2 h for complete hydrolysis, and heated to 90 °C for 5 min. Soluble sugars were analysed by high pH anion exchange chromatography with pulsed amperometric detection (HPAEC-PAD) on a Dionex ICS-5000 system using a DionexCarboPAC™PA-20 column (3×150 mm) with a guard column (3×50 mm) kept at 30 °C and operated at a flow rate of 0.5 ml min^{-1}. The eluents used were (A) 0.1 M sodium hydroxide and (B) 0.1 M sodium hydroxide with 1 M sodium acetate. The gradient used was: 0% (B) from 0 min to 9 min, 10% (B) from 9 min to 10 min, 100% (B) from 10 min to 12 min, and 0% (B) from 12 min to 20 min. Detector temperature was maintained at 20 °C, data collection was at 2 Hz, and the Gold Standard PAD waveform (std. quad. potential) was used. Standards used were: glucose, fructose, sucrose, raffinose, 1-kestose, and nytose at concentrations of 4, 2, 1, 0.5, 0.25, and 0.125 mg l^{-1}, respectively. Total fructan (μM) content was calculated according to Huynh *et al.* (2008) and equals the sum of glucose and fructose after hydrolysis minus the sum of free glucose, fructose, sucrose, and raffinose (before hydrolysis), taking into account the loss of one water molecule per monosaccharide.

Monosaccharide and arabinoxylan analysis

Monosaccharides were analysed following Hassan *et al.* (2017) using reversed phase HPLC separation coupled to diode array detection (Agilent Technologies). Total arabinoxylan content (% w/w) was calculated from the combined amount of % L-arabinose and % D-xylose, taking into account the loss of one water molecule per monosaccharide.

Protein content

The amount of nitrogen in mature grain samples was analysed using the Dumas combustion method following Jung *et al.* (2003). Protein was calculated from the nitrogen content of the material, using a nitrogen conversion factor of 6.25.

RNA isolation and cDNA synthesis

Total RNA was extracted from all tissue homogenates using an Invitrogen™ TRIzol™ (Thermo Fisher Scientific), DNA was removed using a DNA-free kit following the manufacturer's instructions (Ambion®, Thermo Fisher Scientific), and was used as the template for cDNA synthesis following Burton *et al.* (2008).

Real-time quantitative PCR (qPCR)

Gene-specific primers were designed from the 3'-untranslated regions of full-length cDNAs. Fragments amplified using the gene-specific primers were purified using HPLC following Burton *et al.* (2008) and sequenced at the Australian Genome Research Facility, Adelaide, South Australia. PCR primer sequences are provided in Supplementary Table S2 at *JXB* online. qPCR analysis was carried out following Burton *et al.* (2008). Heatmap representation was generated using Multiple Experiment Viewer (MeV) software (http://mev.tm4.org/ accessed 1 October 2019).

Protein extraction, SDS–PAGE, and immunoblotting

Microsomes from frozen barley grain tissues (10 grains each) were isolated according to Song *et al.* (2015). Protein concentration was measured using the BCA protein assay kit (Thermo Fisher Scientific). Protein gel electrophoresis was performed with 30 μg of protein using the NuPAGE Bis-Tris electrophoresis system (Invitrogen) on 4–12% gradient gels (Novex, Life Technologies) with the molecular mass marker Precision Plus Protein Kaleidoscope (BioRad). After electrophoresis, proteins were transferred onto nitrocellulose membrane (Nitrobind, 0.22 μm, Thermo Fisher Scientific) using the XCell II Blot Module (Invitrogen) according to the manufacturer's protocol and processed according to Doblin *et al.* (2009). The membrane was incubated with a polyclonal HvCslF6 primary antibody (Wilson *et al.*, 2015) at 1:2000 dilution followed by anti-rabbit horseradish peroxidase (HRP) conjugate (BioRad) at a 1:10 000 dilution. Signal detection was performed with SuperSignal West Pico chemiluminescent substrate (Thermo Fisher Scientific) according to the manufacturer's instructions and using a ChemiDoc MP Imaging System (BioRad).

Tissue preparation for MALDI-MSI measurement

Sectioning of barley grains and matrix application was performed following Peukert *et al.* (2014). The MS imaging (MSI) measurements were performed using an ultrafleXtreme matrix-assisted laser desorption/ionization (MALDI) time-of-flight (TOF)/TOF device (Bruker Daltonics) following Peukert *et al.* (2016a).

Tissue fixation, embedding, and microscopy for barley grain

Developing grains were halved using a razor blade and fixed in 0.25% glutaraldehyde, 4% paraformaldehyde, and 4% sucrose in phosphate-buffered saline (PBS), pH 7.2, dehydrated, and embedded in LR White resin following Burton *et al.* (2011). Embedded tissue was sectioned (1 μm) on an ultramicrotome using a diamond knife and dried onto polylysine-coated microscope slides (Thermo Fisher Scientific). Immunochemical analysis of cell wall polysaccharides was performed according to Burton *et al.* (2011) using primary antibodies including (1,3)-β-glucan (Biosupplies), hetero-(1,4)-β-mannan (Pettolino *et al.*, 2001), BG1 (Biosupplies), LM11 (McCartney *et al.*, 2005), LM19 (PlantProbes), and a recombinant crystalline cellulose CBM3a protein (PlantProbes). For detection of crystalline cellulose, a monoclonal anti-polyhistidine antibody (Sigma-Aldrich) [1:100 dilution in 1× PBS with 1% (w/v) BSA] was applied after CBM3a (Blake *et al.*, 2006). For detection of arabinoxylan, sections were incubated in α-L-arabinofuranosidase (Megazyme International, Deltagen) under moist conditions at 40 °C for 2 h for unmasking of antibody epitopes prior to LM11 antibody

incubation (Wilson *et al.*, 2012). For detection of homogalacturonan, sections were either not treated or treated with 0.1 M sodium carbonate (Na_2CO_3) for 1 h at room temperature for unmasking of antibody epitopes prior to LM19 antibody incubation (Verhertbruggen *et al.*, 2009). Alexa Fluor® 555 goat anti-mouse IgG (H+L) secondary antibody (Thermo Fisher Scientific) was used against BG1, (1,3)-β-glucan, and anti-polyhistidine antibodies, while Alexa Fluor® 555 goat anti-rat IgG (H+L) secondary antibody (Thermo Fisher Scientific) was used against LM11 and LM19 antibodies. Images were taken using a fluorescence microscope (Axio Imager M2; Carl Zeiss). Tissue sections were stained with Epoxy Tissue Stain 14950 (Proscitech) for morphological examination and were photographed using a Nikon Ni-E optical microscope. For environmental SEM, mature grains were cut in half, mounted on SEM stubs, and examined using an FEI Quanta 450 FEG environmental scanning electron microscope at an accelerating voltage of 10 kV.

Sections were prepared from the equatorial part of the grain. Two biological replicates with two technical replicates of each line were examined.

Aleurone layer dimension and cell shape measurements

To observe the aleurone layer dimensions in mature samples, grains were hand-dissected (transversely) in the mid-region and analysed as described in Aubert *et al.* (2018). Measurements were taken in triplicate from 2–5 sections of three individual grains using a Zeiss M2 AxioImager with an attached AxioCam MrM camera (Zeiss, Germany). Images were analysed using ZEN 2012 software (Zeiss, Germany) at dorsal, left, and right positions. Aleurone layer width was measured as the distance from the edge of the endosperm to the innermost autofluorescent aleurone cell wall. Aleurone proportion was measured by calculating the aleurone area as a percentage of the total endosperm area.

Aleurone cell shape of WT and 18-6 grains was measured similarly from toluidine blue-stained grain sections of 24 DAP grains using ZEN 2012 software from two biological replicates (four sections each). Cell length was defined as the distance from the outward-directed cell wall to the innermost cell wall, while the cell width was measured as the distance from the left-neighbouring-directed cell wall to the right-neighbouring cell wall. In total, 127 and 231 cells were randomly analysed from each line, respectively.

Starch granule size measurements

Ground barley flour was mixed with 1 ml of 2% SDS (Sigma-Aldrich) and 5 µl of 1 M DTT (Sigma-Aldrich) for 10 min. After centrifugation (3000 *g*) for 10 min, the supernatant was decanted. The pellet was washed in 1 ml of Milli-Q water, centrifuged (3000 *g*) for 10 min, and the supernatant decanted. The pellet was suspended in 150 µl of Lugol's iodine solution containing 2% potassium iodine (E. Merck) and 1% iodine (Sigma-Aldrich), and diluted further with 300 µl of Milli-Q water. A drop of the mixed sample was placed on a Bright-Line Hemacytometer (Hausser Scientific); images were taken using a Nikon Ni-E optical microscope. Measurement of starch particles was performed using Image J software (http://imagej.net/Fiji (accessed 1 October 2019)). RGB images were converted to 32 bit black and white format and the default threshold ImageJ settings applied, followed by watershed analysis to separate granules in close physical proximity. Granules were then measured using the 'Analyse particle' function, with size constraints of 1 µm infinity and of 0.8–1.00 circularity. Haemocytometer lines were used to establish scale.

Results

pAsGlo1:HvCslF6 *is expressed in the peripheral endosperm and correlates with increased HvCSLF6 protein and MLG abundance*

To determine HvCSLF6 protein abundance, a specific HvCSLF6 antibody was used (Fig. 1A). Consistent with Wilson *et al.* (2015), a strong doublet of HvCSLF6 protein between 89 kDa and 100 kDa was observed in endosperm extracts of transgenic and WT grain at 15 DAP, although the predicted size for HvCSLF6 is 105 kDa (Wilson *et al.*, 2015). Levels of HvCSLF6 were greater in transgenic endosperm than in the WT; a weak HvCSLF6 signal was also observed in the 18-6 'outer tissues' sample (Fig. 1A). Out of the four transgenic lines tested, the highest accumulation of HvCSLF6 was observed in line 18-6, which also showed the strongest grain morphological phenotype.

Accumulation of *HvCslF6* transcript was measured in WT and transgenic grain tissues at multiple DAP. From 7 to 19 DAP, transcript levels were higher in transgenic 'outer

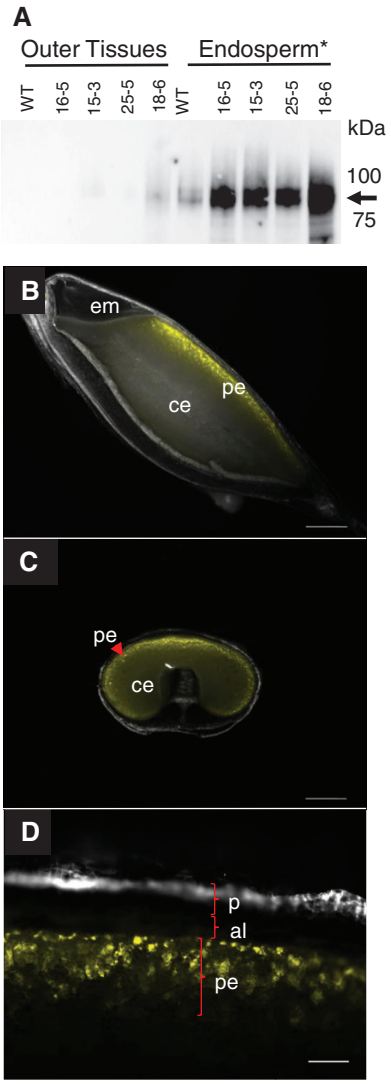

Fig. 1. Detection of HvCslF6 protein and YFP fluorescence in developing barley grain. (A) Total HvCslF6 protein levels in the transgenic grains are slightly higher in 'outer tissues' and clearly higher in endosperm tissues relatively to the WT at 15 DAP. The arrow indicates HvCslF6 protein at 89–100 kDa. (B–D) Fluorescence from YFP is detected in the peripheral endosperm of barley grain at 20 DAP. Images (B) and (C) are under ×1 magnification with scale bars equivalent to 1000 µm. Image (D) is under ×10 magnification with a scale bar equivalent to 100 µm. Sections for image (C) were prepared in the equatorial part of the grain. *Endosperm sample includes embryo tissues. Abbreviations: aleurone (al), central endosperm (ce), embryo (em), pericarp (p), peripheral endosperm (pe).

tissues' and endosperm compared with the WT and WT(tc), and they were also slightly higher in 24 DAP transgenic 'outer tissues' compared with the WT. Lowest expression of the *HvCslF6* transcript was observed for line 15-3. In the embryo, only the 18-6 transgenic line had higher *HvCslF6* transcript levels at 19 DAP relative to the WT (Supplementary Fig. S1A).

To examine tissue specificity of the *AsGlo* promoter (*pAsGlo1*), fresh barley grain sections from plants transformed with the *pAsGlo1:3xnlsYFP* transcriptional fusion construct were observed under a fluorescence microscope. Yellow fluorescent protein (YFP) fluorescence was first detected at ~7 DAP (data not shown) and by 20 DAP was seen specifically in the peripheral endosperm of the grain. No signal was detected in aleurone or pericarp tissues (Fig. 1B–D).

To establish whether contamination from the peripheral endosperm tissue had carried over into the manually prepared 'outer tissues' samples, transcript levels of the aleurone-specific gene, *lipid transfer protein 2* (*HvLtp2*) (Kalla *et al.*, 1994) and the *HvGBSS1a* gene, which is not detectable in barley pericarp (Radchuk *et al.*, 2009), were examined (Supplementary Fig. S1D, E). *HvLtp2* transcript expression was detected at similar levels in both endosperm and 'outer tissues' samples, while Hv*GBSS1a* transcript expression was found at a higher level in endosperm preparations. These results indicate that a considerable proportion of peripheral endosperm was present in the manual preparations of 'outer tissues' of all samples. These samples were named 'outer tissues' throughout the manuscript, and they contained pericarp, testa, nucellar epidermis, and some aleurone cells.

Distribution of MLG was examined by immunolabelling of grain sections (Fig. 2A–D). At 7 DAP, BG1 antibody labelling was evenly detected across both WT and 18-6 transgenic grain (data not shown). At 11 and 24 DAP, signals from BG1 antibody labelling were uniformly distributed across the tissue cell walls in WT grain (Fig. 2A, C) whereas for 18-6 transgenic grain, the fluorescence signals were stronger in the peripheral endosperm cell walls (cell walls appeared thicker; Fig. 2B, D), appearing similar to the *pAsGlo1:3xnlsYFP* expression pattern (Fig. 1C). BG1-associated fluorescence also indicated that peripheral and central endosperm cells in transgenic grain were irregularly arranged and the central endosperm cells appeared more 'squashed' (Fig. 2D). Higher BG1 labelling in transgenic grain coincided with increased endosperm MLG content at 24 DAP (Supplementary Fig. S2A, B) and increased MLG content (% w/w) in the mature endosperm in all transgenic lines compared with the WT (Supplementary Table S1A).

Starch granules are smaller in pAsGlo1:HvCslF6 *transgenic grain*

The 'squashed' endosperm cells in 18-6 transgenic grain were packed with starch granules which appeared smaller than A-type (large) but much larger than B-type granules (small) in the WT (Fig. 3A, B). Small starch granules were also found in the peripheral endosperm layer of 18-6 transgenic grain, while the equivalent cells in the WT contained fewer, larger granules

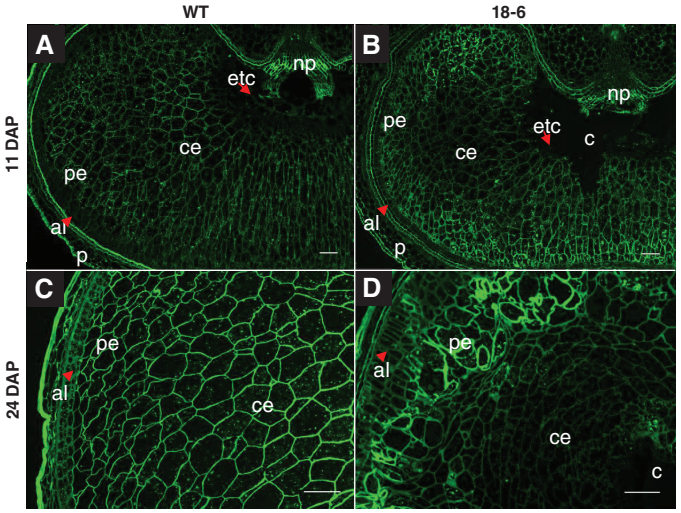

Fig. 2. Immunodetection of (1,3;1,4)-β-glucan in developing barley grain. Labelling with anti-(1,3;1,4)-β-glucan (BG1) monoclonal antibody shows stronger fluorescence signals in the peripheral endosperm of transgenic grain (B) and (D) relative to the WT (A) and (C) at 11 and 24 DAP. (A) and (B) are under ×5 magnification; (C) and (D) are under ×10 magnification. Scale bars are equivalent to 100 μm. Sections were prepared in the equatorial part of the grain for two biological replicates with two technical replicates each. Abbreviations: aleurone (al), cavity (c), central endosperm (ce), endosperm transfer cells (etc), pericarp (p), peripheral endosperm (pe), nucellar projection (np).

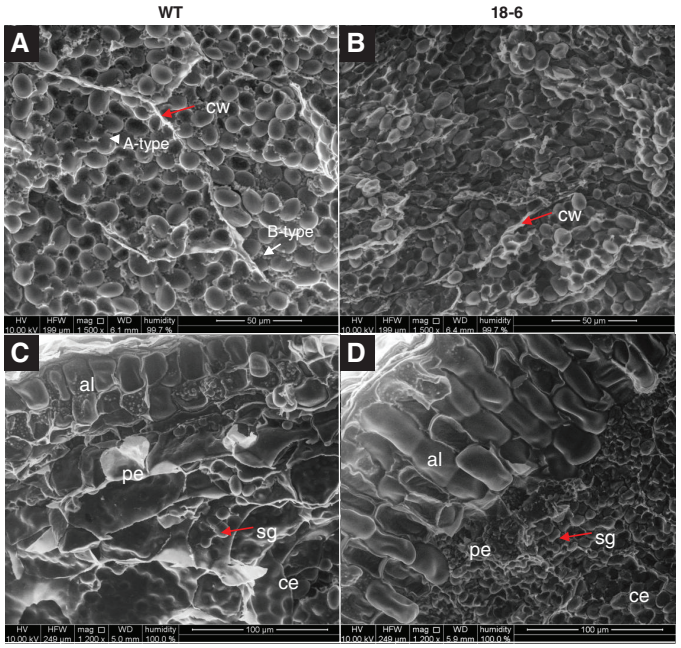

Fig. 3. Environmental scanning electron micrographs of starch granules of mature barley grain. (A) WT endosperm contains A-type (large) and B-type (small) starch granules and the surrounding cell walls are apparent. (B) Starch granules in the 18-6 transgenic endosperm appear packed in an intermediate size between A-type and B-type in the WT grain and the cell walls are less apparent. (C) Aleurone cells in the WT appear cubic, while those of 18-6 transgenic grain appear rectangular cuboid (D). Starch granules are highly packed in the peripheral endosperm layer of 18-6 transgenic grain. (A) and (B) are taken in the distal endosperm regions of grains cross-sectioned in the middle part, viewed at ×1500 magnification with scale bars equivalent to 50 μm. (C) and (D) are taken next to the aleurone layer with ×1200 magnification and scale bars equivalent to 100 μm. Abbreviations: aleurone (al), cell wall (cw), central endosperm (ce), peripheral endosperm (pe), starch granule (sg).

(Fig. 3C, D). The cell walls surrounding the starch granules were more obvious in WT endosperm compared with transgenic endosperm (Fig. 3A, B).

The size and distribution of starch granules in grain from the WT, WT(tc), and all transgenic lines were further examined (Table 1). Barley grain starch comprises large granules with diameters in the range of 10–40 μm and small granules ranging from 1 μm to 10 μm (Palmer, 1972; Chmelik *et al.*, 2001). Therefore, granules with diameters <10 μm were grouped as small granules (B-type) while granules with diameters >10 μm were grouped as large granules (A-type). WT, WT(tc), 15-3, 16-5, and 25-5 had small granules with diameters ranging between 4.3 μm and 4.9 μm, whereas granules from 18-6 had diameters >5 μm. Line 18-6 had the smallest A-type granules, with average diameters of ~15 μm, whereas those of WT, WT(tc), and other transgenic lines ranged between 20 μm and 26 μm. In transgenic grain, the overall size distribution was shifted to a higher proportion of A-type granules while the median granule size in this group was reduced compared with the WT(tc) and WT grain. Lowest effects on starch granules size and distribution were observed for line 15-3 (Table 1).

Abnormal structures of the cavity and ETCs in pAsGlo1:HvCslF6 *transgenic grain*

Similar to each of the other *HvCslF6* transgenic lines, line 18-6 had a smaller endosperm area than the WT due to the presence of the large central cavity (Lim *et al.*, 2018). The ETCs surrounding the central cavity were deformed or sporadically missing. Rupture of ETCs as an artefact of sample preparation can be excluded as this was observed in many different replicates and treatments as well as during cryo-sectioning such as performed for MSI experiments. This phenotype was absent in the WT and WT(tc) grain. We investigated histological changes during the transition phase of grain development (8–14 DAP), where cellularization of transfer tissues has been completed and storage product accumulation starts (Fig. 4A–F; Supplementary Fig. S3A–D). As early as 8 DAP, rupture of tissues adjacent to the nucellar projection (NP), the newly forming cavity, can be observed in transgenic grain while other transfer tissues appear similar to those in the WT (Fig. 4A, B). At 9 DAP, the cavity size in transgenic grain was larger compared with the WT, and the ETCs showed irregular cell types while the cavity surrounding the cell layer remained intact (Supplementary Fig. S3A, B).

Table 1. *Analysis of starch granules in mature barley grain*

	WT	WT(tc)	F6-15-3	F6-16-5	F6-18-6	F6-25-5
	Average diameter of starch granules					
A-type large granules (>10 μm)	22.99±0.71	25.77±0.65*	22.34±0.99	20.64±0.68*	15.24±0.41*	20.45±0.25*
B-type small granules (<10 μm)	4.60±0.12	4.93±0.02*	4.51±0.12	4.29±0.21*	5.49±0.12*	4.39±0.05*
	Distribution given as % of granules falling into the respective bins					
1–2.5 μm	7.38±1.44	5.87±1.81	7.38±1.03	10.40±3.62	7.27±3.20	8.16±1.20
2.5–5 μm	46.15±4.38	40.62±2.20	46.79±5.67	32.50±4.41	17.11±2.85	29.94±4.33
5–7.5 μm	31.01±3.68	36.93±3.09	28.84±3.29	14.35±1.84	15.92±1.26	13.21±1.54
7.5–10 μm	5.461.09	7.76±1.23	4.43±0.82	5.43±1.21	14.63±1.04	5.62±0.96
Total % small	90.01	91.17	87.43	62.69	54.92	56.94
10–12.5 μm	0.88±0.22	1.05±0.20	1.18±0.58	3.89±0.93	13.67±1.62	4.43±0.59
12.5–15 μm	0.61±0.22	0.34±0.06	1.01±0.60	4.19±0.89	11.90±1.65	4.51±0.42
15–17.5 μm	0.71±0.35	0.33±0.10	1.14±0.70	4.50±1.59	8.11±0.74	5.08±0.87
17.5–20 μm	0.96±0.49	0.45±0.16	1.32±0.82	5.01±1.14	5.38±1.54	6.17±1.18
20–22.5 μm	1.33±0.64	0.55±0.19	1.68±0.98	5.51±1.19	3.03±1.04	7.10±1.25
22.5–25 μm	1.47±0.71	0.75±0.43	1.75±0.98	5.02±1.50	1.57±0.35	5.94±1.32
25–27.5 μm	1.43±0.55	1.00±0.44	1.63±0.64	4.01±0.79	0.70±0.34	4.35±1.04
27.5–30 μm	1.16±0.39	1.08±0.50	1.25±0.53	2.38±0.57	0.45±0.14	2.95±1.01
30–32.5 μm	0.72±0.24	1.10±0.53	0.76±0.31	1.64±0.39	0.17±0.11	1.46±0.38
32.5–35 μm	0.42±0.16	0.85±0.38	0.48±0.19	0.66±0.27	0.07±0.06	0.68±0.23
35–37.5 μm	0.19±0.10	0.57±0.36	0.21±0.11	0.32±0.15	0.02±0.02	0.26±0.14
37.5–40 μm	0.08±0.04	0.40±0.37	0.09±0.04	0.10±0.13	0.002±0.007	0.08±0.07
40–42.5 μm	0.02±0.02	0.19±0.16	0.03±0.02	0.07±0.11	0	0.03±0.03
42.5–45 μm	0.01±0.01	0.11±0.08	0.02±0.02	0.01±0.02	0	0.01±0.02
45–47.5 μm	0.004±0.01	0.04±0.03	0.003±0.006	0.02±0.04	0	0
47.5–50 μm	0	0.02±0.02	0.003±0.006	0	0	0
>50 μm	0	0.01±0.02	0.001±0.001	0	0	0
Total % large	9.99	8.83	12.57	37.31	45.08	43.06

The number of evaluated granules per sample varied between 1588 and 21 193; three biological replicates with three technical replicates each were analysed per line. The average diameter of starch granules, grouped into large (A-type, >10 μm) and small (B-type, <10 μm) granules, ± SD is shown in the upper part of the table. An asterisk indicates a significant difference from the WT by *t*-test with *P*-values of <0.05. The distribution based on the diameter of starch granules is given in the lower part of the table as % ±SD of granules falling into the respective size categories. A grey scale (dark grey, highest value; white, lowest value) has been applied to highlight the most abundant size proportion within the groups of A- and B-type granules, and the overall percentage of granules per group is given for each line.

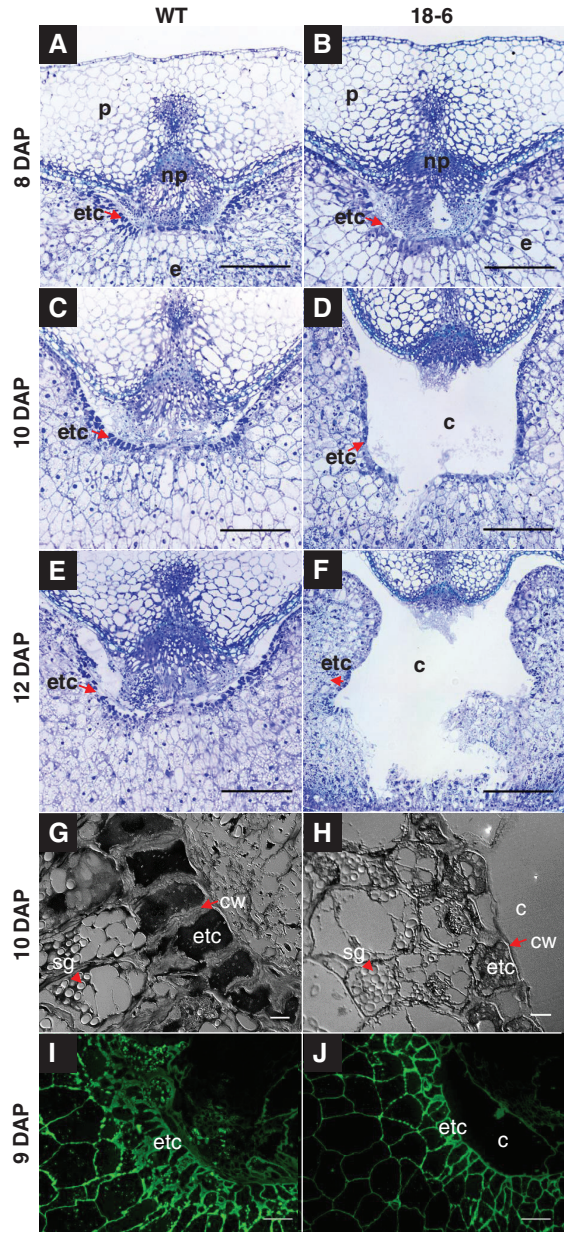

Fig. 4. Histological images of the ventral crease region in WT and transgenic (18-6) barley grain. The endosperm transfer cells (ETCs) in the WT appear intact (A, C, and E) while the ETCs in transgenic grain are poorly formed in the region adjacent to the emerging cavity and start to be disrupted during the early storage phase (B, D, and F). ETCs in WT grain are denser with thicker cell walls (G) compared with loosely organized ETCs with thinner cell walls in transgenic grain (H) at 10 DAP. (I) and (J) Immunodetection of mannan [(1–4)-β-D-mannan and galacto-(1–4)-β-D-mannan antibody] revealed stronger fluorescence in the cell walls of WT ETCs relative to transgenic grain at 9 DAP. (A–F) Toluidine blue-stained grain sections under ×4 magnification; scale bars=100 μm. (G) and (H) ×60 magnification; scale bars=10 μm. (I) and (J) ×20 magnification; scale bars=50 μm. Abbreviations: cavity (c), cell wall (cw), endosperm (e), endosperm transfer cell (etc), nucellar projection (np), pericarp (p), starch granule (sg).

At 10 DAP, the ETCs in transgenic grain were ruptured (Fig. 4C, D), becoming increasingly pronounced during subsequent development, whereas the ETCs remained intact in the WT grain (Fig. 4E, F; Supplementary Fig. S3C, D). In WT grain, cell walls of the ETCs were denser and thicker (Fig. 4G) compared with those of transgenic grain which were thinner and surrounded by much less regularly shaped cells (Fig. 4H).

Altered cell wall composition in the ETCs and endosperm of pAsGlo1:HvCslF6 *transgenic grain*

To determine whether ETC rupture might be associated with changes in cell wall composition, sections of WT and 18-6 transgenic grain were examined. From 9 to 11 DAP, the labelling patterns for the mannan antibody were similar between WT and transgenic grain, although the intensity of mannan labelling was higher in the WT (Fig. 4I, J). Labelling of MLG (Fig. 2A, B), callose (Supplementary Fig. S4A, B), crystalline cellulose (Supplementary Fig. S4C, D), and arabinoxylan (Supplementary Fig. S5A, B) was not detected in the ETC walls of either WT or transgenic grain. Arabinoxylan labelling was greater in the nucellar epidermis of transgenic grain when compared with the WT (Supplementary Fig. S5A, B). Labelling of pectin was detected in the cell walls of the NP, and notably only in the walls of ETCs adjacent to the cavity in both transgenic and WT grain (Supplementary Fig. S6A–D).

Clear differences were observed in the abundance of arabinoxylan, crystalline cellulose, and callose in the endosperm walls of WT and 18-6 grain (Supplementary Fig. S5A–H) where transgenic grain showed stronger labelling for arabinoxylan and callose relative to the WT (Supplementary Fig. S5A–D). More intense labelling for callose and crystalline cellulose was detected in the peripheral endosperm of transgenic grains relative to the WT, similar to MLG (Fig. 2A–D; Supplementary Fig. S5C–F). Labelling of crystalline cellulose was completely absent in the nucellar epidermis and adjacent cell rows of transgenic grain (Supplementary Fig. S5E, F), as noted for ETCs (Supplementary Fig. S4C, D). The labelling intensity of mannan (Supplementary Fig. S5G, H) was similar between WT and transgenic endosperm, as was that of LM19, which was detected in maternal grain tissues following pretreatment with 0.1 M sodium carbonate (Supplementary Fig. S6E–H).

Modified aleurone cell shape in pAsGlo1:HvCslF6 *transgenic grain*

At 9 DAP, peripheral endosperm cells in 18-6 and WT grain appeared similarly developed (Supplementary Fig. S7A, B), while at 12–14 DAP, aleurone cells in 18-6 appeared larger relative to the WT (Supplementary Fig. S7C–F). By 24 DAP, they were notably elongated in 18-6 while the equivalent WT cells remained cube shaped (Supplementary Fig. S7G, H). From 14 to 24 DAP, increasing thickness of 18-6 aleurone and peripheral endosperm cell walls was observed relative to the WT (Supplementary Fig. S7E–H) coinciding with increased MLG, arabinoxylan, callose, and cellulose deposition in these cell walls (Fig. 2C, D; Supplementary Fig. S5A–F).

Measuring aleurone cell shape revealed that at 24 DAP, the average length in 18-6 was 44.8±0.2 μm (SE) and the width was 16.1±0.3 μm (SE). For the WT, the average length was 18.7±0.5 μm (SE) with a width of 17.8±0.2 μm (SE), confirming that WT aleurone cells were cuboid and transgenic

cells were over twice as long as, but similar in width to, those of the WT. Transgenic aleurone cells remained relatively elongated inwardly compared with the WT at each stage through to grain maturity (Fig. 3D), and the aleurone layer was thicker at maturity in all transgenic lines relative to the WT (Supplementary Fig. S8).

pAsGlo1:HvCslF6 *transgenic barley grain accumulated more (1,3;1,4)-β-glucan, sucrose, and total fructan, and less starch in the endosperm compared with the WT*

Storage carbohydrate deposition was examined in WT, WT(tc), and transgenic lines from 7 DAP until maturity (Fig. 5A–F). Differences were observed in the MLG content of the WT(tc) lines relative to the WT, whereas the levels of starch, sucrose, and total fructan were similar (Fig. 5A, B; Supplementary Table S1A). Likewise, with the transgenic lines, the greatest variations were observed in 18-6 and the smallest in 15-3, which had similar levels of MLG to WT(tc) per grain but significantly lower levels of starch. WT and WT(tc) grain accumulated starch and MLG throughout grain development (Fig. 5A, B), whilst starch and MLG declined slightly after 24 DAP in transgenic grain (Fig. 5C–F). WT and WT(tc) grain reached maximum total fructan levels at 11 DAP at ~1.2 mg, while transgenic lines ranged between 1.2 mg and 1.5 mg from 11 to 24 DAP (Fig. 5C–F). Sucrose levels in WT and WT(tc) grain were constant from 11 DAP to maturity at 0.5 mg, and increased in transgenic grain from 11 to 19 DAP, from 0.7 mg to 1 mg (Fig. 5C–F). MLG levels were increased in transgenic developing grain from 11 DAP onwards relative to the WT. At maturity on a per grain basis, transgenic grain (except line 16-5 with similar and line 18-6 with lower MLG levels) contained more MLG but less starch than WT grain (Fig. 5; Supplementary Table S1A). While glucose and fructose levels were lower in all transgenic grain samples, sucrose and total fructan levels were comparable with those of the WT and WT(tc) (Supplementary Table S1A). On a weight per weight basis, all transgenic grain contained more MLG, sucrose, and total fructan (except line 15-3 with similar total fructan levels) but less starch than the WT in developing and mature endosperm (Supplementary Figs S2A, C, S9A, C; Supplementary Table S1A). Protein levels were reduced in grain of all transgenic lines on a per grain basis, which is mainly attributed to the reduced endosperm weight relative to WT and WT(tc) grain (Supplementary Table S1). The fraction of other grain constituents, including lipids, cellulose, lignin, and other secondary metabolites (e.g. tocopherol and phytosterols), minerals, and vitamins was higher in mature 'outer tissues' and endosperm of transgenic grain (Supplementary Table S1A). Cellulose is likely to be the major component of the grain cell wall, as shown in Supplementary Fig. S5E and F.

Sucrose and fructans accumulate in the developing pAsGlo1:HvCslF6 *grain*

Drastic morphological changes in transgenic ETCs coincided with the early phase of storage product formation (9–14 DAP) (Fig. 4A–F; Supplementary Fig. S3A–D), and were followed by pronounced differences in endosperm storage product accumulation from 15 DAP onwards (Fig. 5A–F; Supplementary Figs S2A–D, S9A–D). MALDI-MSI was used to visualize the spatio-temporal distribution of oligosaccharides in WT and 18-6 transgenic grain at both 15 and 24 DAP. Sections were prepared from basal grain parts to also observe the embryo region (Fig. 6A–H). At 15 DAP, accumulation of disaccharides [degree of polymerization 2 (DP2)] in transgenic and WT cavity regions was similar (Fig. 6C), while signals for trisaccharides (DP3) and tetrasaccharides (DP4) were higher in transgenic endosperm and between the endosperm and embryo (Fig. 6E, G). At 24 DAP, DP2 levels were comparable in the cavity and embryo of both transgenic and WT grain (Fig. 6D), whilst DP3 and DP4 signals remained higher in the transgenic grain, mainly adjacent to the cavity and endosperm (Fig. 6F, H).

Quantitative measurement of soluble sugars in cavity fluids revealed that glucose, fructose, sucrose, and total fructan levels, as a proportion of the total sugars from one whole grain, were similar between WT and transgenic grain at 11 DAP (Table 2). At 15 DAP, glucose, sucrose, and total fructan levels increased significantly in the transgenic cavity compared with the WT (Table 2), with transgenic sucrose and total fructan levels still higher at 24 DAP (Table 2). At 15 DAP, twice as much volume of cavity fluid was obtained from transgenic lines compared with WT grain (Supplementary Fig. S11).

Carbohydrate metabolic pathways are altered in pAsGlo1:HvCslF6 *grain*

Transcript levels of genes encoding key enzymes associated with carbohydrate synthesis and encoding proteins with carbohydrate transport roles were measured in 'outer tissues', endosperm, and embryo across development. The genes were cell wall-related [*HvCslF6*, *HvCslH1*, *endo-β-(1,3;1,4)-glucanase E1* (*Endo E1*), *cellulose synthase 2* (*CesA2*), and *cellulose synthase-like F9* (*CslF9*)], starch-related [*GBSS1a*, *starch synthase 2* (*SS 2*), *SBE2a*, *SBE2b*, *Iso1*, *LD*, and *sucrose synthase1* (*SuSy1*)], sucrose metabolism-related [*cell wall invertase 1* (*CWINV1*), *vacuolar invertase* (*VIN*), *sucrose phosphate synthase* (*SPS*), *sucrose phosphate phosphatase* (*SPP*), *sucrose transporter 1* (*SUT1*), and *sucrose transporter 2* (*SUT2*)], and fructan biosynthetic genes (*1-SST*, *1-FFT*, and *6-SFT*). *HORVU6Hr1G011260* (*INV**) and *HORVU2Hr1G109120* (*INV***) were selected based on their putative role in hydrolysing glycosidic bonds between two carbohydrate molecules, including fructans (Fig. 7; Supplementary Table S2).

Consistent with increased expression from the *pAsGlo1:HvCslF6* construct, *HvCslF6* transcript was up-regulated in transgenic endosperm at 7 and 11 DAP, declining until 24 DAP, whilst *HvCslH1* was up-regulated in transgenic endosperm from 15 to 24 DAP (Fig. 7). In embryo tissues, *HvCslF6* was up-regulated at 19 DAP. *Endo E1*, encoding a protein that hydrolyses MLG, was down-regulated in transgenic endosperm and embryo across development (Fig. 7). *HvCslF9*, encoding another MLG synthase with the highest expression at ~8 DAP in developing grain (Burton *et al.*,

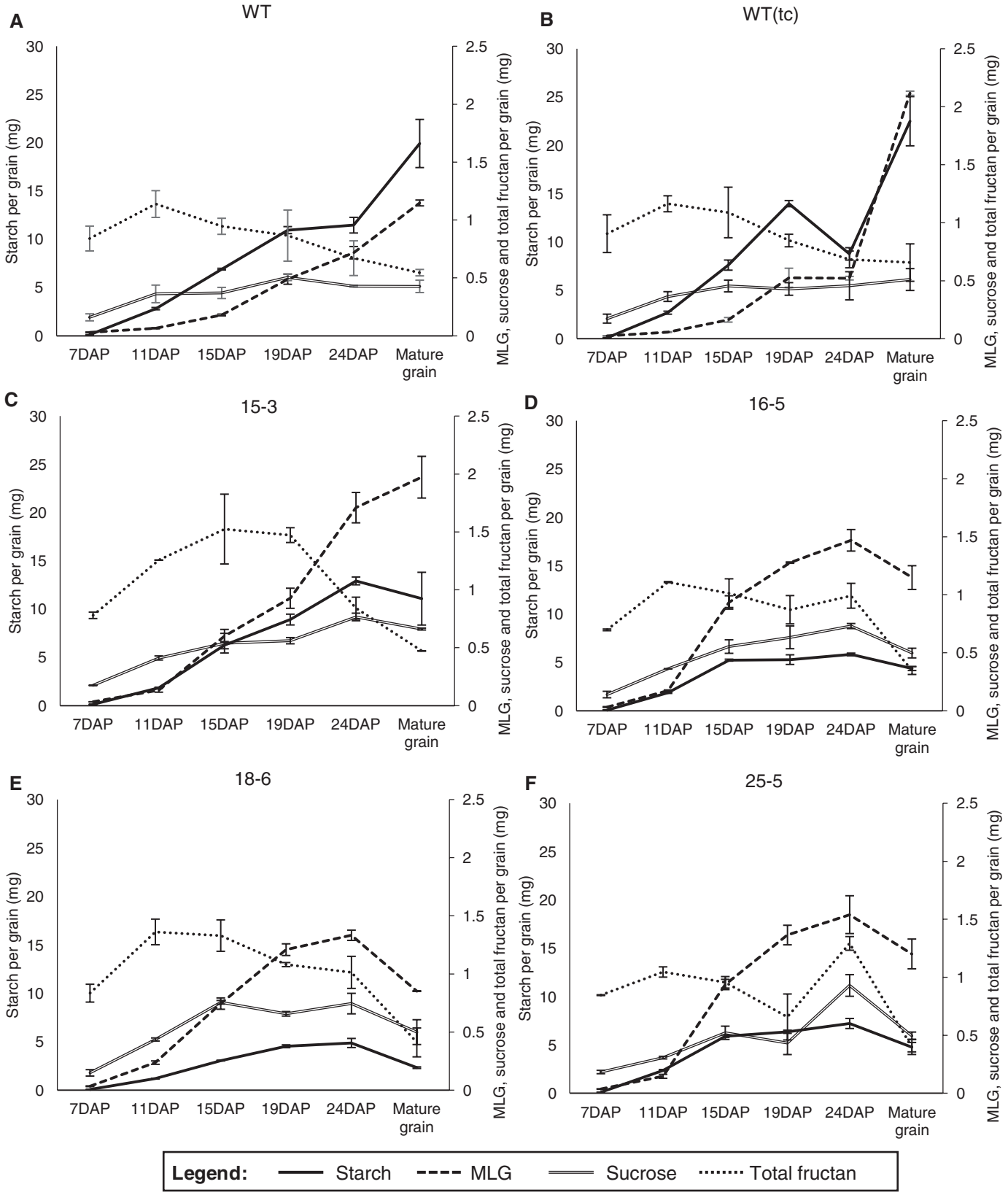

Fig. 5. The carbohydrate content: MLG, starch, sucrose, and total fructan during barley grain development on a per grain basis (mg). (A) WT, (B) WT(tc), and *pAsGlo1:HvCslF6* transgenic lines (C) 15-3, (D) 16-5, (E) 18-6, and (F) 25-5. For measurements of storage carbohydrates (MLG and starch) from developing and mature grains, 'outer tissues' and endosperm were analysed as a single sample. The embryo, containing low amounts of storage carbohydrates, was removed and used for analysis of soluble sugars. For soluble sugar measurements, developing and mature grains were separated into 'outer tissues', endosperm, and embryo. The total sum of values is shown. Additional carbohydrate content and statistics for mature grain are presented in Supplementary Table S1 for 'outer tissues' plus endosperm as well as for embryo tissues and in Supplementary Figs S2, S9, and S10 for developing grain tissues.

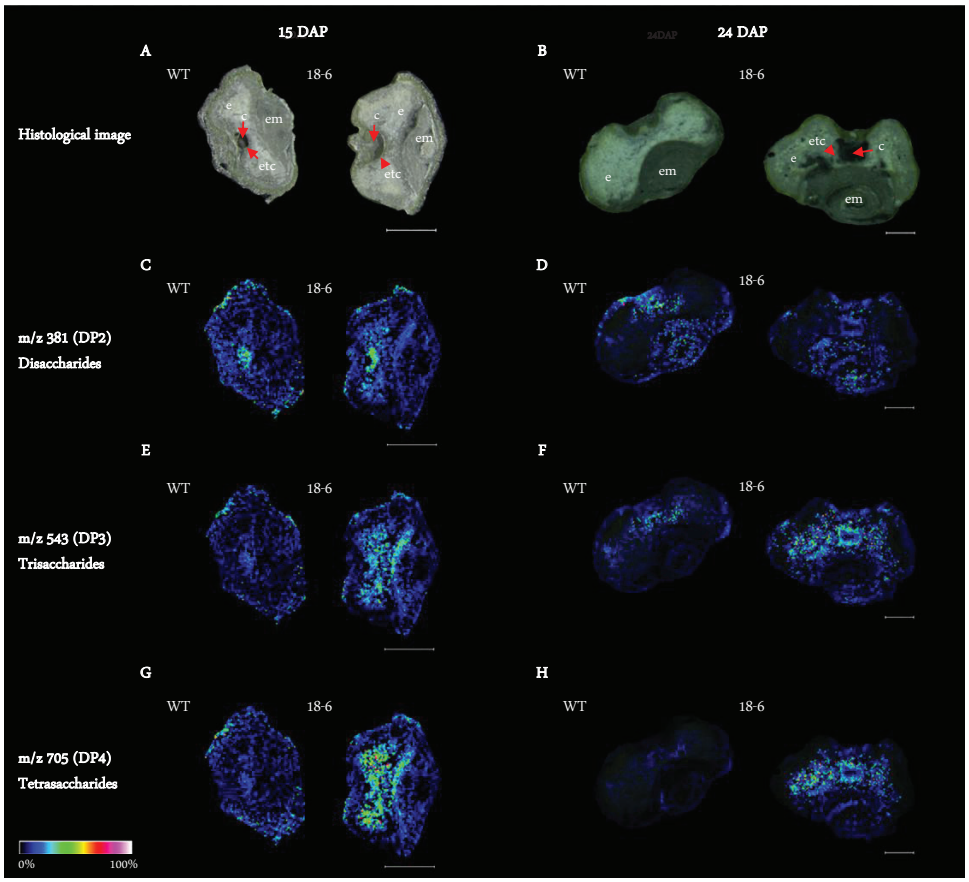

Fig. 6. Visualization of oligosaccharides in WT and 18-6 transgenic grain at 15 and 24 DAP using a MALDI-MSI approach. (A) and (B) are histological images of WT and transgenic grain at 15 and 24 DAP, respectively. (C) At 15 DAP, disaccharides (DP2) are mostly accumulated in and around the endosperm cavity of WT and transgenic grain. (D) At 24 DAP, DP2 signal intensity is highest in the endosperm cavity and embryo of WT and transgenic grain. (E) and (G) show stronger signal intensities of trisaccharides (DP3) and tetrasaccharides (DP4) in the endosperm and tissues adjacent to the embryo of transgenic grain relative to the WT at 15 DAP. (F) and (H) show stronger signal intensities of DP3 and DP4 in the endosperm and endosperm cavity of transgenic grain relative to the WT at 24 DAP. Scale bars in (A), (C), (E), and (G) are equivalent to 500 µm. Scale bars in (B), (D), (F), and (H) are equivalent to 200 µm. Sections were prepared in the basal part of the grain. Colours used in the single ion intensity maps correspond to signal intensity scaling displayed at the bottom right. Abbreviations: cavity (c), embryo (em), endosperm (e), endosperm transfer cell (etc).

2008), was down-regulated in transgenic endosperm from 7 to 15 DAP relative to the WT (Supplementary Fig. S1B) while *HvCesA2*, encoding a cellulose synthase (Burton *et al.*, 2004; Desprez *et al.*, 2007), showed similar transcript levels in both WT and transgenic endosperm from 7 to 15 DAP and was down-regulated from 19 to 24 DAP (Supplementary Fig. S1C).

Starch metabolic gene transcripts, *SS2*, *SBE2a*, *SBE2b*, *GBSS1a*, *Iso1*, and *LD*, were down-regulated in transgenic endosperm across development, with the lowest levels at 24 DAP. In contrast, *SBE1* was highly up-regulated compared with the WT in all transgenic tissues during development (Fig. 7). Sucrose is hydrolysed by cell wall invertase (*CWINV*) and vacuolar invertase (*VIN*). *CWINV1* was down-regulated in transgenic endosperm and embryo during late grain filling from 19 to 24 DAP. In the fructan metabolic pathway, *6-SFT* was up-regulated in the transgenic endosperm from 11 to 19 DAP and in the embryo slightly at 19 DAP, while *6-SFT*, *1-SST*, and *1-FFT* were all increased during late grain filling from 19 to 24 DAP relative to the WT (Fig. 7). The *HORVU2Hr1G109120* gene was up-regulated concurrently with the *6-SFT* gene in transgenic endosperm, while *HORVU6Hr1G011260* transcript levels changed oppositely to *6-SFT* (Fig. 7).

The sucrose transporter gene, *SUT1*, was up-regulated in transgenic endosperm at 19 DAP and down-regulated in transgenic embryo at 15 DAP, while *SUT1* and *SUT2* were both slightly up-regulated in transgenic 'outer tissues' at 24 DAP relative to the WT. *SuSy1*, *SPS*, and *SPP*, all involved in sucrose metabolism, showed only small transcript changes compared with the WT (Fig. 7). During the storage phase overall (15–24 DAP), fructan biosynthetic and sucrose transporter genes were up-regulated, whilst invertase and starch metabolic genes were down-regulated in the transgenic endosperm, coinciding with increased sucrose and fructans and decreased starch contents, as shown in the sugar quantitative data (Supplementary Figs S2C, D, S9A, C, D).

Discussion

Specificity of pAsGlo1 *promoter activity in barley grain and* HvCslF6 *regulation*

Increased endosperm MLG content in *pAsGlo1:HvCslF6* lines is consistent with the early activity of the *pAsGlo1* promoter shortly after the completion of endosperm cellularization

Table 2. *Percentage of soluble sugar content (glucose, fructose, sucrose, and total fructan) in the endosperm cavity per total corresponding sugar from a single grain at 11, 15, and 24 DAP on a w/w basis*

	Glucose (%w/w) ±SD			Fructose(%w/w) ±SD			Sucrose(%w/w) ±SD			Total fructan(%w/w) ±SD		
	DAP			DAP			DAP			DAP		
	11	15	19	11	15	19	11	15	19	11	15	19
WT	0.33±0.01	0.40±0.32	0.48±0.27	0.26±0.02	0.17±0.13	0.24±0.18	0.26±0.02	0.19±0.09	0.02±0.03	0.32±0.02	0.22±0.14	0.06±0.06
WT (tc)	0.23±0.18	0.37±0.41	0.66±0.79	0.17±0.14	0.28±0.32	0.35±0.44	0.16±0.13	0.03±0.03*	0.02±0.01	0.20±0.16	0.07±0.02*	0.10±0.02
15-3	0.50±0.34	0.75±0.00*	0.94±0.54	0.24±0.18	0.17±0.00	0.33±0.24	0.42±0.29	0.47±0.05*	0.31±0.20*	0.51±0.39	0.52±0.09*	0.60±0.34*
16-5	0.31±0.25	0.84±0.09*	0.85±0.62	0.22±0.18	0.28±0.03	0.28±0.19	0.30±0.16	0.82±0.07*	0.15±0.03*	0.39±0.27	0.81±0.11*	0.39±0.13*
18-6	0.27±0.20	1.04±0.72*	0.19±0.02*	0.13±0.06*	0.72±0.66	0.18±0.08	0.25±0.17	0.52±0.14*	0.08±0.00*	0.28±0.16	0.75±0.29*	0.14±0.03*
25-5	0.10±0.07*	0.82±0.08*	0.83±0.23	0.07±0.06*	0.27±0.07	0.25±0.07	0.13±0.13*	0.57±0.06*	0.24±0.05*	0.13±0.12*	0.63±0.06*	0.58±0.17*

An asterisk indicates a significant difference from the WT by *t*-test with *P*-values of <0.05.

(Wilson *et al.*, 2006), specifically in the peripheral endosperm and matching the up-regulation of *HvCslF6* transcripts at 7 DAP (Fig 1A–D; Supplementary Fig. S1A). The *pAsGlo1*-driven YFP was not detected in transgenic 'outer tissues' or embryo, so higher *HvCslF6* transcript levels here may be due to contamination from the peripheral endosperm layer. Similar contamination arising from hand dissection of grain tissues has been reported for endosperm transcriptome data sets (Schon and Nodine, 2017). Based on these observations, we assume that *HvCslF6* transgene overexpression occurs exclusively in the endosperm, and not in the 'outer tissues' or embryo.

Previous studies have indicated that regulation of MLG synthesis, and *HvCSlF6* transcript levels can change in response to varying environmental conditions (Dickin *et al.*, 2011; and reviewed in Houston *et al.*, 2016). Consistent with these previous observations, here we observed that wild type lines that had been through tissue culture [WT(tc)] were similar to the WT in relation to their grain starch, sucrose, and total fructan, but they differed in the MLG content, indicating that there may be feedback from the environmental cues that can influence the regulation of *HvCslF6* in grain. Differences in *HvCslF6* expression (Supplementary Fig. S1A) are also likely to be the reason for the variation between transgenic lines in their grain MLG, starch, sucrose, and total fructan levels (Fig. 5; Supplementary Table S1).

Altered aleurone development in pAsGlo1:HvCslF6 *transgenic barley*

The aleurone cells in 18-6 transgenic grain appeared permanently elongated inwardly by 24 DAP (Fig. 3C, D; Supplementary Fig. S7A–H). Differentiation of aleurone cells is initiated at ~8 DAP (Bosnes *et al.*, 1992) driven by signals released from the peripheral starchy endosperm (Becraft and Asuncion-Crabb, 2000; Gruis *et al.*, 2006). A number of genes are involved in regulating aleurone cell fate and tissue differentiation in cereal grains, including *defective kernel1* (*Dek1*), *crinkly4* (*Cr4*), and *supernumerary aleurone1* (*Sal1*) (Lid *et al.*, 2002; Olsen *et al.*, 2008). Aleurone development is also associated with hormonal regulation (Bethke *et al.*, 1999; Gómez-Cadenas *et al.*, 2001; Geisler-Lee and Gallie, 2005) whilst aleurone cell number has been linked to endosperm and embryo development as well as to differential hydrolytic enzyme activity (Aubert *et al.*, 2018). For example, *disorgal* maize mutants have more aleurone cells, a shrunken endosperm with reduced starch granule density, and a smaller embryo (Lid *et al.*, 2004); *defective seed5* (*des5*) barley mutants have fewer aleurone cells, a shrunken endosperm, and altered starch granule types, and embryos prematurely abort (Olsen *et al.*, 2008).

Peripheral endosperm cells containing more *HvCslF6* transcript and HvCslF6 protein appear to be structurally different from the WT from 9 DAP onwards (Figs 2A–D, 3A–D). The thicker cell walls in transgenic aleurone (Fig. 4E–H) relative to the WT probably result from an extended period of MLG deposition in the peripheral endosperm cells, as also shown for *Brachypodium distachyon* (Trafford *et al.*, 2013). Due to the specific grain size, cell expansion is only possible towards the middle of the grain, resulting in inwardly elongated aleurone cells and 'squeezed' adjacent starchy endosperm.

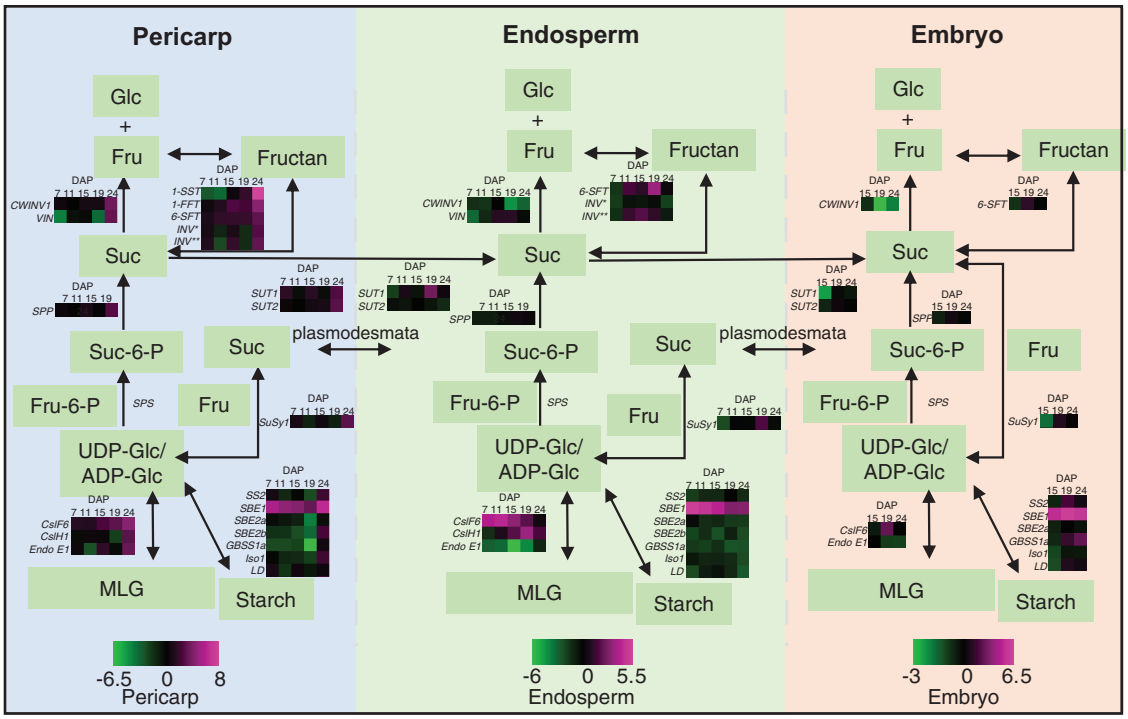

Fig. 7. Schematic diagram of the carbohydrate metabolic pathway in 'outer tissues', endosperm, and embryo of a barley grain and the differential transcript expression of involved genes in 18-6 transgenic grain from 7 to 24 DAP. Expression of *HvCslF6* transcripts includes the transgene and wild-type (WT) gene expression. For each tissue, the transcript expression values are normalized against the WT, calculated as log2, and represented in a heat map. Genes where the maximum transcript value was <2000 arbitrary units were not included in the heat map. Vertical dashed lines separate the three grain tissues. UDP-glucose (UDP-Glc) and ADP-glucose (ADP-Glc) are substrates for the biosynthesis of (1,3;1,4)-β-glucan and starch, respectively. INV* indicates the *HORVU6Hr1G011260* gene. INV** indicates the *HORVU2Hr1G109120* gene, which are both involved in the hydrolysis of glycosidic bonds between the carbohydrates, including fructans. Abbreviations: fructose (Fru), fructose-6-phosphate (Fru-6-P), glucose (Glc), sucrose (Suc), sucrose-6-phosphate (Suc-6-P). Expanded gene names and accession information is included in Supplementary Table S2. Magenta indicates increased expression, while green indicates decreased expression.

Morphology and cell wall composition changes in pAsGlo1:HvCslF6 *ETCs*

A larger cavity and unevenly formed ETC layer were observed in transgenic grain relative to the WT from 9 DAP onwards, and the ETCs began to rupture at 10 DAP (Fig. 4C, D; Supplementary Fig. S3A, B). At this stage, the ETC walls in transgenic grain showed less intense mannan labelling than the WT (Fig. 4I, J). In the ETC walls, no MLG, arabinoxylan, callose, or crystalline cellulose was detected (Supplementary Fig. S5A–D), while the labelling of pectin probably relates to the remnants from the nucellus (Supplementary Fig. S6–H) (Greenwood *et al.*, 2005).

These results do not match the transcriptome analysis by Thiel *et al.* (2012), who demonstrated up-regulation of genes related to callose and cellulose metabolism at the same time point (10 DAP). The failure of antibodies to detect cell wall polysaccharides other than mannan could be due to epitope masking, making them unavailable for binding, as has been reported by Xue *et al.* (2013). Closer examination of the cell wall polysaccharides in ETCs may be achieved using immunogold labelling and TEM, with appropriate unmasking techniques. Alternatively, laser microdissection of the ETCs and surrounding endosperm would allow examination of gene expression and link it directly to cell wall composition.

Altered ETC morphology may trigger abnormal accumulation of sucrose and fructans in the grain cavity and endosperm

Correct formation of ETCs is important to ensure nutrient transfer from the cavity to the endosperm for development and storage of carbohydrates. A study by Felker *et al.* (1985) showed that some barley mutants with abnormal endosperm had missing ETCs, such as *seg2*, *seg4*, *seg5*, and *seg8*, and starch filling in the endosperm was also perturbed. Here, in *HvCslF6* transgenic grain during the early storage phase, a significant increase in glucose, sucrose, and fructan content in the cavity and endosperm compared with the WT was observed, whilst starch levels were reduced (Figs 5C–F, 6C–H; Table 2; Supplementary Figs S2C, S9A–D, S11A–D). We hypothesize that the high sucrose and fructan pools in the cavity at 15 DAP may be due to earlier perturbations in ETC differentiation, which may have subsequently perturbed the active flow of sucrose towards the endosperm. A link between changed carbohydrate partitioning and altered development of the transfer region has been suggested previously (Vijn and Smeekens, 1999; Weichert *et al.*, 2010; Ruan, 2014). However, a detailed histological examination of ETC development in *pAsGlo1:HvCslF6* grain is required to confirm changes in ETC identity and function. In contrast, the *lys5* mutant Risø13, harbouring a mutation in the plastidial ADP-glucose

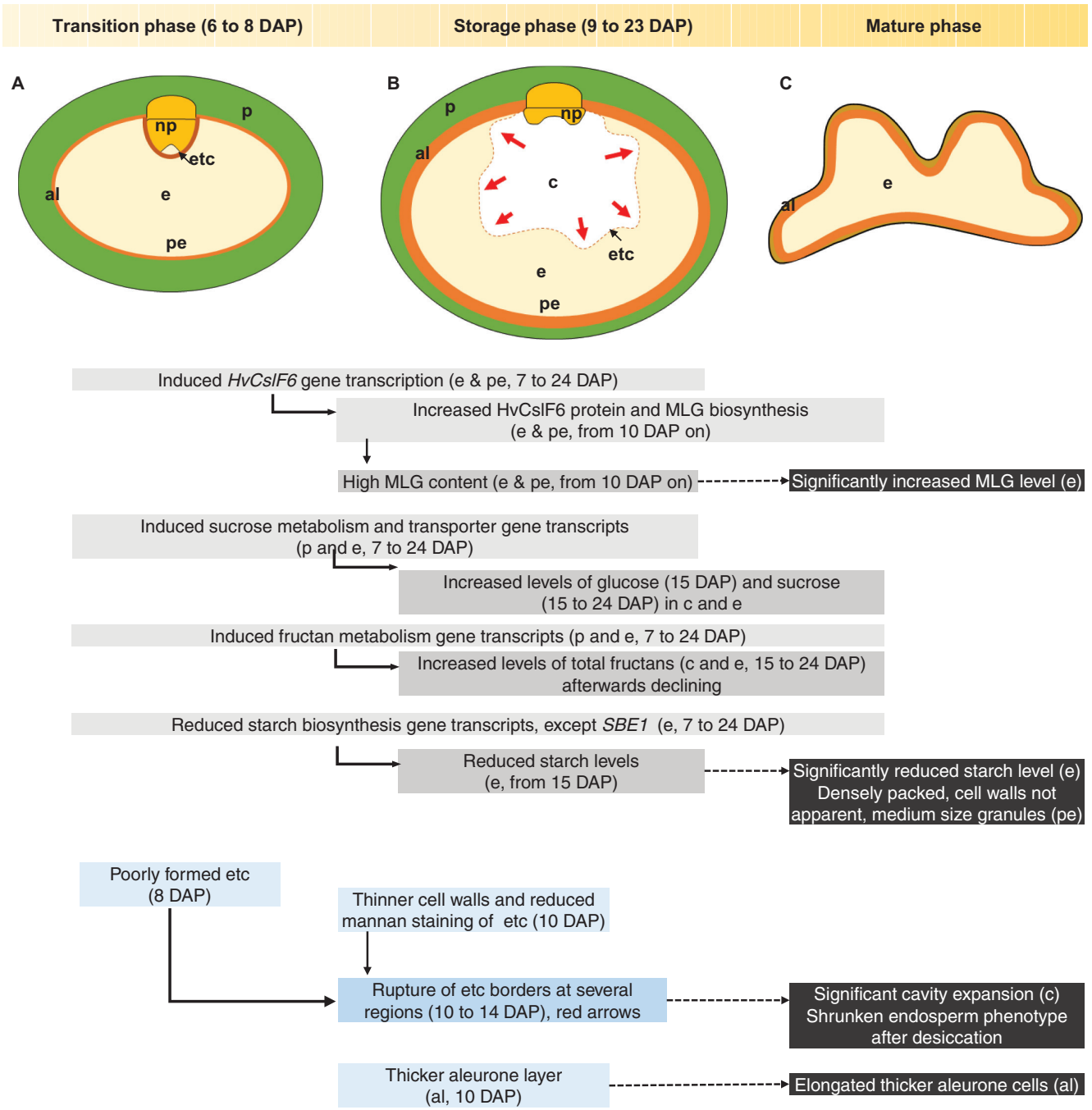

Fig. 8. Schematic diagram of grain development of the *pAsGlo1:HvCslF6* transgenic line (A–C) relative to the wild type. (A) In transgenic endosperm, the early up-regulation of *HvCslF6* gene expression relative to the WT from 7 DAP results in an increased amount of (1,3;1,4)-β-glucan (MLG) during the grain storage phase, which is followed by a decreased amount of starch and increased levels of glucose, sucrose, and total fructans. Early changes in carbohydrate biosynthesis allocation appear to influence endosperm transfer cell (ETC) differentiation and subsequently perturb sucrose uptake in the endosperm. (B) Consequently, high amounts of sucrose and fructans are accumulated in the grain cavity, causing the cavity to aberrantly expand and subsequent rupture (as indicated by the dotted line). Thinner cell walls in the non-uniformly developed ETCs of transgenic grain and variations in mannan labelling may contribute to ETC rupture in transgenic grain. (C) The transgenic grain has an elongated aleurone layer compared with the WT grain which persisted to maturity. As the grain matures, fluid in the transgenic cavity dries out, causing the grain to become shrunken. High levels of MLG and low levels of starch persist in the mature endosperm. Abbreviations: aleurone (al), cavity (c), endosperm (e), endosperm transfer cells (etc), nucellar projection (np), pericarp (p), peripheral endosperm (pe). Red arrows indicate probable osmotic pressure exerted from the cavity towards the endosperm. Grey boxes indicate findings at the genetic and metabolic level, while blue boxes indicate findings at the morphological level. Dark grey boxes highlight the mature phenotype. Arrangement of boxes roughly reflects observation time during the course of grain development.

transporter resulting in reduced starch biosynthesis, did not show such morphological changes or spatial alterations of the sucrose allocation, but decreased velocity of the sucrose stream through the cavity, as compared with the WT (Melkus *et al*., 2011). Thus, the wrinkled phenotype of mature Risø13 grains is possibly associated with decreased starch deposition in the endosperm and the strongly altered starch granule morphology (Patron *et al*., 2004).

Fructans in the endosperm cavity are involved in detoxification of hydroxyl radicals (Peukert *et al.*, 2014; Matros *et al.*, 2015) and maintaining the sucrose gradient between the vascular bundle and sink tissues (Pollock and Cairns, 1991; Peukert *et al.*, 2016b). In 18-6 transgenic grain, ETCs were irregularly formed and the sucrose uptake pathway was likely to have been compromised. At the same time, the increased demand for glucose during MLG synthesis in the endosperm would be likely to have stimulated sucrose import. Fructan synthesis can be induced by sucrose (Vijn and Smeekens, 1999; Ruan, 2014), towards keeping the levels of free fructose temporarily low. In the transgenic endosperm, the fructosyltransferase gene, *6-SFT*, is up-regulated, encoding an enzyme catalysing the formation of branched and levan-type fructans containing β(2,6) linkages (Vijn and Smeekens, 1999). Down-regulation of *CWINV1* and *VIN* in the transgenic endosperm may also contribute to the increased amounts of sucrose and fructan, and small amounts of free glucose.

Starch metabolism is perturbed in pAsGlo1:HvCslF6 *endosperm*

pAsGlo1:HvCslF6 grain showed up-regulation of the glucan synthase *HvCslH1* and down-regulation of the endo-glucanase *E1* in the developing endosperm (Fig. 7), probably resulting from increased abundance of metabolic precursors and constitutively induced MLG synthesis, respectively. High MLG content in barley is likely to be balanced by lower starch levels as previously reported (Munck *et al.*, 2004; Seefeldt *et al.*, 2009; Burton *et al.*, 2011) and, as seen here, linked to the down-regulation of some starch biosynthetic genes (Fig. 7). This coincides with results from *B. distachyon* where MLG accumulated as the main storage carbohydrate in cell walls during grain development at the expense of starch in mature grain (Guillon *et al.*, 2011). The low capacity for starch synthesis in *Brachypodium* is reflected by reduced transcription of *SS1* and *SBE1* as well as reduced activity of starch synthase and ADP-glucose pyrophosphorylase (Trafford *et al.*, 2013). In our study, *SBE1* was up-regulated in transgenic endosperm. Previously, SBE1 was found to be involved in producing long-chain amylopectin in rice (Satoh *et al.*, 2003) and in maize (reviewed in Tetlow and Emes, 2014). However, alterations in amylopectin chain length have not been investigated in our study and it is unclear whether up-regulation of *SBE1* contributes to overall starch granule size differences seen in barley (Fig. 3A, B; Table 1). Recently, RNAi suppression of all three HvSBE isoforms was shown to result in a severe amylose-only phenotype with irregular granules, while hyperphosphorylation caused WT-like structures (Shaik *et al.*, 2016). Further investigations need to include the amylose/amylopectin ratio and starch phosphorylation status in *pAsGlo1:HvCslF6* grain.

Conclusions

Increased MLG levels are desirable for human health benefits, but high levels in barley grain from early stages perturb carbohydrate metabolism, leading to impairment in grain development (Fig. 8). Major changes affect the cell wall composition and morphology of the peripheral endosperm regions (aleurone and adjacent endosperm cells), and, notably, of the ETC layer. The increased MLG synthesis in transgenic grain is compromised by reduced starch and increased fructan synthesis. The high demand for maternally derived sucrose together with the disturbed active import to the endosperm via the ETC border probably result in excessive accumulation of sucrose and fructans in the cavity. The shrunken phenotype of the *HvCslF6* transgenic grain is likely to be due to the increased amount of cavity fluids and higher osmotic potential, forcing water uptake and causing wrinkling due to greater water loss during desiccation. Our investigations of the metabolic, transcriptional, and morphological changes associated with increasing MLG early in grain development (this report) or systemically (Burton *et al.*, 2011) have shown the importance of regulation of carbohydrate metabolism homeostasis in controlling grain phenotypes, suggesting that these transgenic approaches may not be an ideal avenue in pursuit of this outcome. Engineering of barley lines with MLG synthesis inducible at the grain-filling stage as well as selection for high MLG lines from available barley mutant collections may overcome these limitations in the near future.

Supplementary data

Supplementary data are available at *JXB* online.

Fig. S1. Normalized transcript levels of *HvCslF6* transgene, *HvCslF9*, *HvCesA2*, *HvLtp2*, and *HvGBSS1a* in developing grain tissues.

Fig. S2. MLG and starch contents in developing grain.

Fig. S3. Morphology of the endosperm cavity in WT and 18-6 transgenic grain at 9 and 14 DAP.

Fig. S4. Immunohistochemical analysis of callose and crystalline cellulose in ETC walls at 10 DAP.

Fig. S5. Immunohistochemical analysis of arabinoxylan, callose, crystalline cellulose, and mannan in endosperm cell walls at 10 DAP.

Fig. S6. Immunohistochemical analysis of pectins with LM19 antibody on barley grain sections at 10 DAP.

Fig. S7. Morphology of aleurone cells in developing WT and 18-6 transgenic grain.

Fig. S8. Morphology of aleurone cells in WT and 18-6 transgenic grain at grain maturation and during grain development.

Fig. S9. Sucrose and total fructan contents in developing rain.

Fig. S10. Percentage of soluble glucose and fructose contents in developing grain on a w/w and per grain basis (mg).

Fig. S11. Total volume of fluids in the endosperm cavity.

Table S1. Carbohydrate content in mature grain (embryo removed) and embryo.

Table S2. List of primers used for real-time PCR.

Acknowledgments

The authors wish to acknowledge Dr Wei Zeng (University of Melbourne), Dr Gwenda Mayo, Dr Lisa O'Donovan, and Ken Neubauer (Adelaide Microscopy, University of Adelaide), Dr Rohan Singh, Katherine Allder, and Kylie Neumann (University of Adelaide) for their technical assistance,

and Dr Hans-Peter Mock (Leibniz Institute of Plant Genetics and Crop Plant Research, for stimulating discussions. This work was supported by an Adelaide Graduate Research Scholarship (AGRS), the Australian Research Council (ARC) Centre of Excellence in Plant Cell Walls (CE110001007), ARC Fellowship funding (DE150100837 and FT140100780), a German Academic Exchange Service (DAAD) G08 Australia Germany Exchange Program, and a grant by the German Research Foundation (DFG, MA 4814/3-1) to AM. All authors state that they have no conflict of interest concerning this manuscript.

References

Åman P, Hesselman K, Tilly AC. 1985. The variation in chemical composition of Swedish barleys. Journal of Cereal Science **3**, 73–77.

Aubert MK, Coventry S, Shirley NJ, Betts NS, Würschum T, Burton RA, Tucker MR. 2018. Differences in hydrolytic enzyme activity accompany natural variation in mature aleurone morphology in barley (*Hordeum vulgare* L.). Scientific Reports **8**, 11025.

Becraft PW, Asuncion-Crabb Y. 2000. Positional cues specify and maintain aleurone cell fate in maize endosperm development. Development **127**, 4039–4048.

Bethke PC, Lonsdale JE, Fath A, Jones RL. 1999. Hormonally regulated programmed cell death in barley aleurone cells. The Plant Cell **11**, 1033–1046.

Blake AW, McCartney L, Flint JE, Bolam DN, Boraston AB, Gilbert HJ, Knox JP. 2006. Understanding the biological rationale for the diversity of cellulose-directed carbohydrate-binding modules in prokaryotic enzymes. Journal of Biological Chemistry **281**, 29321–29329.

Bosnes M, Weideman F, Olsen OA. 1992. Endosperm differentiation in barley wild-type and sex mutants. The Plant Journal **2**, 661–674.

Burton RA, Collins HM, Kibble NA, *et al*. 2011. Over-expression of specific HvCslF cellulose synthase-like genes in transgenic barley increases the levels of cell wall (1,3;1,4)-β-D-glucans and alters their fine structure. Plant Biotechnology Journal **9**, 117–135.

Burton RA, Fincher GB. 2012. Current challenges in cell wall biology in the cereals and grasses. Frontiers in Plant Science **3**, 130.

Burton RA, Fincher GB. 2014. Evolution and development of cell walls in cereal grains. Frontiers in Plant Science **5**, 456, 1–15.

Burton RA, Jobling SA, Harvey AJ, Shirley NJ, Mather DE, Bacic A, Fincher GB. 2008. The genetics and transcriptional profiles of the cellulose synthase-like HvCslF gene family in barley. Plant Physiology **146**, 1821–1833.

Burton RA, Shirley NJ, King BJ, Harvey AJ, Fincher GB. 2004. The CesA gene family of barley. Quantitative analysis of transcripts reveals two groups of co-expressed genes. Plant Physiology **134**, 224–236.

Carciofi M, Blennow A, Jensen SL, Shaik SS, Henriksen A, Buléon A, Holm PB, Hebelstrup KH. 2012. Concerted suppression of all starch branching enzyme genes in barley produces amylose-only starch granules. BMC Plant Biology **12**, 223.

Chmelik J, Krumlová A, Budinská M, Kruml T, Psota V, Bohacenko I, Mazal P, Vydrová H. 2001. Comparison of size characterization of barley starch granules determined by electron and optical microscopy, low angle laser light scattering and gravitational field-flow fractionation. Journal of the Institute of Brewing **107**, 11–17.

Clarke B, Liang R, Morell MK, Bird AR, Jenkins CL, Li Z. 2008. Gene expression in a starch synthase IIa mutant of barley: changes in the level of gene transcription and grain composition. Functional & Integrative Genomics **8**, 211–221.

Curtis MD, Grossniklaus U. 2003. A gateway cloning vector set for high-throughput functional analysis of genes in planta. Plant Physiology **133**, 462–469.

Desprez T, Juraniec M, Crowell EF, Jouy H, Pochylova Z, Parcy F, Höfte H, Gonneau M, Vernhettes S. 2007. Organization of cellulose synthase complexes involved in primary cell wall synthesis in *Arabidopsis thaliana*. Proceedings of the National Academy of Sciences, USA **104**, 15572–15577.

Dickin E, Steele K, Frost G, Edwards-Jones G, Wright D. 2011. Effect of genotype, environment and agronomic management on β-glucan concentration of naked barley grain intended for health food use. Journal of Cereal Science **54**, 44–52.

Doblin MS, Pettolino FA, Wilson SM, Campbell R, Burton RA, Fincher GB, Newbigin E, Bacic A. 2009. A barley cellulose synthase-like CSLH gene mediates (1,3;1,4)-beta-D-glucan synthesis in transgenic Arabidopsis. Proceedings of the National Academy of Sciences, USA **106**, 5996–6001.

Domínguez F, Cejudo FJ. 2014. Programmed cell death (PCD): an essential process of cereal seed development and germination. Frontiers in Plant Science **5**, 366.

Felker FC, Peterson DM, Nelson OE. 1985. Anatomy of immature grains of eight maternal effect shrunken endosperm barley mutants. American Journal of Botany **72**, 248–256.

Fincher GB. 1975. Morphology and chemical composition of barley endosperm cell walls. Journal of the Institute of Brewing **81**, 116–122.

Geisler-Lee J, Gallie DR. 2005. Aleurone cell identity is suppressed following connation in maize kernels. Plant Physiology **139**, 204–212.

Gómez-Cadenas A, Zentella R, Walker-Simmons MK, Ho T-HD. 2001. Gibberellin/abscisic acid antagonism in barley aleurone cells: site of action of the protein kinase PKABA1 in relation to gibberellin signaling molecules. The Plant Cell **13**, 667–679.

Greenwood JS, Helm M, Gietl C. 2005. Ricinosomes and endosperm transfer cell structure in programmed cell death of the nucellus during *Ricinus* seed development. Proceedings of the National Academy of Sciences, USA **102**, 2238–2243.

Gruis DF, Guo H, Selinger D, Tian Q, Olsen OA. 2006. Surface position, not signaling from surrounding maternal tissues, specifies aleurone epidermal cell fate in maize. Plant Physiology **141**, 898–909.

Guillon F, Bouchet B, Jamme F, Robert P, Quéméner B, Barron C, Larré C, Dumas P, Saulnier L. 2011. *Brachypodium distachyon* grain: characterization of endosperm cell walls. Journal of Experimental Botany **62**, 1001–1015.

Hassan AS, Houston K, Lahnstein J, Shirley N, Schwerdt JG, Gidley MJ, Waugh R, Little A, Burton RA. 2017. A genome wide association study of arabinoxylan content in 2-row spring barley grain. PLoS One **12**, e0182537.

Henry R, Saini H. 1989. Characterization of cereal sugars and oligosaccharides. Cereal Chemistry **66**, 362–365.

Henry RJ. 1988. The carbohydrates of barley grains—a review. Journal of the Institute of Brewing **94**, 71–78.

Hrmova M, Fincher GB. 2001. Structure–function relationships of beta-D-glucan endo- and exohydrolases from higher plants. Plant Molecular Biology **47**, 73–91.

Houston K, Tucker MR, Chowdhury J, Shirley N, Little A. 2016. The plant cell wall: a complex and dynamic structure as revealed by the responses of genes under stress conditions. Frontiers in Plant Science **7**, 984.

Huynh BL, Palmer L, Mather DE, Wallwork H, Graham RD, Welch RM, Stangoulis JCR. 2008. Genotypic variation in wheat grain fructan content revealed by a simplified HPLC method. Journal of Cereal Science **48**, 369–378.

Jeon JS, Ryoo N, Hahn TR, Walia H, Nakamura Y. 2010. Starch biosynthesis in cereal endosperm. Plant Physiology and Biochemistry **48**, 383–392.

Jung S, Rickert D, Deak N, Aldin E, Recknor J, Johnson L, Murphy P. 2003. Comparison of Kjeldahl and Dumas methods for determining protein contents of soybean products. Journal of the American Oil Chemists' Society **80**, 1169–1173.

Kalla R, Shimamoto K, Potter R, Nielsen PS, Linnestad C, Olsen OA. 1994. The promoter of the barley aleurone-specific gene encoding a putative 7 kDa lipid transfer protein confers aleurone cell-specific expression in transgenic rice. The Plant Journal **6**, 849–860.

Keeling PL, Myers AM. 2010. Biochemistry and genetics of starch synthesis. Annual Review of Food Science and Technology **1**, 271–303.

Kohorn BD, Kobayashi M, Johansen S, Riese J, Huang LF, Koch K, Fu S, Dotson A, Byers N. 2006. An Arabidopsis cell wall-associated kinase required for invertase activity and cell growth. The Plant Journal **46**, 307–316.

Lid SE, Al RH, Krekling T, Meeley RB, Ranch J, Opsahl-Ferstad HG, Olsen OA. 2004. The maize disorganized aleurone layer 1 and 2 (dil1, dil2)

mutants lack control of the mitotic division plane in the aleurone layer of developing endosperm. Planta **218**, 370–378.

Lid SE, Gruis D, Jung R, Lorentzen JA, Ananiev E, Chamberlin M, Niu X, Meeley R, Nichols S, Olsen OA. 2002. The defective kernel 1 (dek1) gene required for aleurone cell development in the endosperm of maize grains encodes a membrane protein of the calpain gene superfamily. Proceedings of the National Academy of Sciences, USA **99**, 5460–5465.

Lim WL, Collins HM, Singh RR, Kibble NAJ, Yap K, Taylor J, Fincher GB, Burton RA. 2018. Method for hull-less barley transformation and manipulation of grain mixed-linkage beta-glucan. Journal of Integrative Plant Biology **60**, 382–396.

Little A, Schwerdt JG, Shirley NJ, *et al*. 2018. Revised phylogeny of the cellulose synthase gene superfamily: insights into cell wall evolution. Plant Physiology **177**, 1124–1141.

Matros A, Peshev D, Peukert M, Mock HP, Van den Ende W. 2015. Sugars as hydroxyl radical scavengers: proof-of-concept by studying the fate of sucralose in Arabidopsis. The Plant Journal **82**, 822–839.

McCartney L, Marcus SE, Knox JP. 2005. Monoclonal antibodies to plant cell wall xylans and arabinoxylans. Journal of Histochemistry and Cytochemistry **53**, 543–546.

McCleary B, Solah V, Gibson T. 1994. Quantitative measurement of total starch in cereal flours and products. Journal of Cereal Science **20**, 51–58.

McCleary BV, Codd R. 1991. Measurement of (1→3),(1→4)-β-D-glucan in barley and oats: a streamlined enzymic procedure. Journal of the Science of Food and Agriculture **55**, 303–312.

Melkus G, Rolletschek H, Fuchs J, *et al*. 2011. Dynamic $^{13}C/^{1}H$ NMR imaging uncovers sugar allocation in the living seed. Plant Biotechnology Journal **9**, 1022–1037.

Munck L, Møller B, Jacobsen S, Søndergaard I. 2004. Near infrared spectra indicate specific mutant endosperm genes and reveal a new mechanism for substituting starch with (1→3,1→4)-β-glucan in barley. Journal of Cereal Science **40**, 213–222.

Nemeth C, Andersson AA, Andersson R, Mangelsen E, Sun C, Åman P. 2014. Relationship of grain fructan content to degree of polymerisation in different barleys. Food and Nutrition Sciences **5**, 581–598.

Olsen LT, Divon HH, Al R, Fosnes K, Lid SE, Opsahl-Sorteberg HG. 2008. The defective seed5 (des5) mutant: effects on barley seed development and *HvDek1*, *HvCr4*, and *HvSal1* gene regulation. Journal of Experimental Botany **59**, 3753–3765.

Olsen OA. 2001. Endosperm development: cellularization and cell fate specification. Annual Review of Plant Biology **52**, 233–267.

Palmer GH. 1972. Morphology of starch granules in cereal grains and malts. Journal of the Institute of Brewing, **78**, 326–332.

Patron NJ, Greber B, Fahy BF, Laurie DA, Parker ML, Denyer K. 2004. The lys5 mutations of barley reveal the nature and importance of plastidial ADP-Glc transporters for starch synthesis in cereal endosperm. Plant Physiology **135**, 2088–2097.

Pettolino FA, Hoogenraad NJ, Ferguson C, Bacic A, Johnson E, Stone BA. 2001. A (1→4)-beta-mannan-specific monoclonal antibody and its use in the immunocytochemical location of galactomannans. Planta **214**, 235–242.

Peukert M, Lim WL, Seiffert U, Matros A. 2016*a*. Mass spectrometry imaging of metabolites in barley grain tissues. Current Protocols in Plant Biology **1**, 574–591.

Peukert M, Thiel J, Mock HP, Marko D, Weschke W, Matros A. 2016*b*. Spatiotemporal dynamics of oligofructan metabolism and suggested functions in developing cereal grains. Frontiers in Plant Science **6**, 1245.

Peukert M, Thiel J, Peshev D, Weschke W, Van den Ende W, Mock HP, Matros A. 2014. Spatio-temporal dynamics of fructan metabolism in developing barley grains. The Plant Cell **26**, 3728–3744.

Pollock CJ, Cairns AJ. 1991. Fructan metabolism in grasses and cereals. Annual Review of Plant Physiology and Plant Molecular Biology **42**, 77–101.

Radchuk VV, Borisjuk L, Sreenivasulu N, Merx K, Mock HP, Rolletschek H, Wobus U, Weschke W. 2009. Spatiotemporal profiling of starch biosynthesis and degradation in the developing barley grain. Plant Physiology **150**, 190–204.

Ruan YL. 2014. Sucrose metabolism: gateway to diverse carbon use and sugar signaling. Annual Review of Plant Biology **65**, 33–67.

Satoh H, Nishi A, Yamashita K, Takemoto Y, Tanaka Y, Hosaka Y, Sakurai A, Fujita N, Nakamura Y. 2003. Starch-branching enzyme I-deficient mutation specifically affects the structure and properties of starch in rice endosperm. Plant Physiology **133**, 1111–1121.

Schon MA, Nodine MD. 2017. Widespread contamination of arabidopsis embryo and endosperm transcriptome data sets. The Plant Cell **29**, 608–617.

Seefeldt HF, Blennow A, Jespersen BM, Wollenweber B, Engelsen SB. 2009. Accumulation of mixed linkage (1→3)(1→4)-β-D-glucan during grain filling in barley: a vibrational spectroscopy study. Journal of Cereal Science **49**, 24–31.

Shaik SS, Obata T, Hebelstrup KH, Schwahn K, Fernie AR, Mateiu RV, Blennow A. 2016. Starch granule re-structuring by starch branching enzyme and glucan water dikinase modulation affects caryopsis physiology and metabolism. PLoS One **11**, e0149613.

Song L, Zeng W, Wu A, *et al*. 2015. Asparagus spears as a model to study heteroxylan biosynthesis during secondary wall development. PLoS One **10**, e0123878.

Sreenivasulu N, Borisjuk L, Junker BH, Mock HP, Rolletschek H, Seiffert U, Weschke W, Wobus U. 2010. Barley grain development toward an integrative view. International Review of Cell and Molecular Biology **281**, 49–89.

Tetlow IJ, Emes MJ. 2014. A review of starch-branching enzymes and their role in amylopectin biosynthesis. IUBMB Life **66**, 546–558.

Thiel J, Riewe D, Rutten T, Melzer M, Friedel S, Bollenbeck F, Weschke W, Weber H. 2012. Differentiation of endosperm transfer cells of barley: a comprehensive analysis at the micro-scale. The Plant Journal **71**, 639–655.

Trafford K, Haleux P, Henderson M, Parker M, Shirley NJ, Tucker MR, Fincher GB, Burton RA. 2013. Grain development in *Brachypodium* and other grasses: possible interactions between cell expansion, starch deposition, and cell-wall synthesis. Journal of Experimental Botany **64**, 5033–5047.

Ueda M, Zhang Z, Laux T. 2011. Transcriptional activation of Arabidopsis axis patterning genes WOX8/9 links zygote polarity to embryo development. Developmental Cell **20**, 264–270.

Verhertbruggen Y, Marcus SE, Haeger A, Ordaz-Ortiz JJ, Knox JP. 2009. An extended set of monoclonal antibodies to pectic homogalacturonan. Carbohydrate Research **344**, 1858–1862.

Verspreet J, Pollet A, Cuyvers S, Vergauwen R, Van den Ende W, Delcour JA, Courtin CM. 2012. A simple and accurate method for determining wheat grain fructan content and average degree of polymerization. Journal of Agricultural and Food Chemistry **60**, 2102–2107.

Vickers CE, Xue G, Gresshoff PM. 2006. A novel cis-acting element, ESP, contributes to high-level endosperm-specific expression in an oat globulin promoter. Plant Molecular Biology **62**, 195–214.

Vijn I, Smeekens S. 1999. Fructan: more than a reserve carbohydrate? Plant Physiology **120**, 351–360.

Wagner W, Wiemken A. 1986. Properties and subcellular localization of fructan hydrolase in the leaves of barley (*Hordeum vulgare* L. cv Gerbel). Journal of Plant Physiology **123**, 429–439.

Weichert N, Saalbach I, Weichert H, *et al*. 2010. Increasing sucrose uptake capacity of wheat grains stimulates storage protein synthesis. Plant Physiology **152**, 698–710.

Wilson SM, Burton RA, Collins HM, Doblin MS, Pettolino FA, Shirley N, Fincher GB, Bacic A. 2012. Pattern of deposition of cell wall polysaccharides and transcript abundance of related cell wall synthesis genes during differentiation in barley endosperm. Plant Physiology **159**, 655–670.

Wilson SM, Burton RA, Doblin MS, Stone BA, Newbigin EJ, Fincher GB, Bacic A. 2006. Temporal and spatial appearance of wall polysaccharides during cellularization of barley (*Hordeum vulgare*) endosperm. Planta **224**, 655–667.

Wilson SM, Ho YY, Lampugnani ER, Van de Meene AM, Bain MP, Bacic A, Doblin MS. 2015. Determining the subcellular location of synthesis and assembly of the cell wall polysaccharide (1,3;1,4)-β-D-glucan in grasses. The Plant Cell **27**, 754–771.

Wobus U, Sreenivasulu N, Borisjuk L, Rolletschek H, Panitz R, Gubatz S, Weschke W. 2005. Molecular physiology and genomics of developing barley grains. Recent Research Developments in Plant Molecular Biology **2**, 1–29.

Xue J, Bosch M, Knox JP. 2013. Heterogeneity and glycan masking of cell wall microstructures in the stems of *Miscanthus* × *giganteus*, and its parents *M. sinensis* and *M. sacchariflorus*. PLoS One **8**, e82114.